

CHARACTERIZATION OF CONDUCTING POLYMERS OF
ESTER LINKAGE CONTAINING THIOPHENE DERIVATIVES
VIA MASS SPECTROSCOPY

A THESIS SUBMITTED TO
THE GRADUATE SCHOOL OF NATURAL AND APPLIED SCIENCES
OF
MIDDLE EAST TECHNICAL UNIVERSITY

BY

EVREN ASLAN

IN PARTIAL FULFILLMENT OF THE REQUIREMENTS FOR THE DEGREE OF
MASTER OF SCIENCE

IN
CHEMISTRY

DECEMBER 2004

Approval of the Graduate School of Natural and Applied Sciences.

Prof. Dr. Canan Özgen

Director

I certify that this thesis satisfies all the requirements as a thesis for the degree of Master of Sciences.

Prof. Dr. Hüseyin İşçi

Head of the Department

This is to certify that we have read this thesis and that in our opinion it is fully adequate, in scope and quality, as a thesis for the degree of Master of Sciences.

Prof. Dr. Jale Hacaloğlu

Co-Supervisor

Prof. Dr. Levent Toppare

Supervisor

Examining Committee Members

Prof. Dr. Leyla Aras (METU, CHEM)

Prof. Dr. Levent Toppare (METU, CHEM)

Prof. Dr. Jale Hacaloğlu (METU, CHEM)

Prof. Dr. Duygu Kısakürek (METU, CHEM)

Prof. Dr. Mustafa Güllü (Ankara University, CHEM)

I hereby declare that all information in this document has been obtained and presented in accordance with academic rules and ethical conduct. I also declare that, as required by these rules and conduct, I have fully cited and referenced all material and results that are not original to this work.

Name, Last name : Evren ASLAN

Signature :

ABSTRACT

CHARACTERIZATION OF CONDUCTING POLYMERS OF ESTER LINKAGE CONTAINING THIOPHENE DERIVATIVES VIA MASS SPECTROSCOPY

Aslan, Evren

M.Sc., Department of Chemistry

Supervisor: Prof. Dr. Levent Toppare

Co-Supervisor: Prof.Dr. Jale Hacaloğlu

December 2004, 86 pages

In order to investigate the thermal and structural characteristics of terephthalic acid bis-(2-thiophen-3-yl-ethyl)ester (TATE), decanedioic acid bis-(2-thiophen-3-yl- ethyl) ester (DATE) and octanoic acid 2-thiophen-3-yl-ethyl ester (OTE), their corresponding homopolymers, copolymers with thiophene and polythiophene, pyrolysis mass spectrometry technique was utilized. The results were discussed in detail considering the effects of spacer group in between ester linkages. Thermal Gravimetry Analysis was used to investigate the weight loss for polymers and monomers. Conductivities of samples were measured by four-probe technique.

It was found that when the ester linkages contain hydrocarbon chains, the growth of polymer occurred through both 2 and 5 positions. On the other hand, when the ester linkages contain more rigid groups such as phenyl, steric hindrance inhibited the growth of the polymer through 2- position and polymerization proceeded via coupling of thiophene moieties mainly at 5-position yielding a polymer with lower conductivity. Though the structure of P(OTE) is inherently different than P(DATE) and P(TATE) extent of network structure is also quite low for this polymer compared to PTh.

Similar thermal characterizations were recorded indicating that thermal units were not significantly affected by the presence of TATE, DATE or OTE for all copolymer samples.

Keywords: electropolymerization, pyrolysis, polythiophene, thermal degradation, mass spectrometry

ÖZ

ESTER BAĞI İÇEREN TİYOFEN TÜREVİ İLETKEN POLİMERLERİN KÜTLE SPEKTROKOPİSİ İLE KARAKTERİZASYONU

Aslan, Evren

Yüksek Lisans, Kimya Bölümü

Tez Yöneticisi: Prof. Dr. Levent Toppare

Ortak Tez Yöneticisi: Prof.Dr. Jale Hacaloğlu

Aralık 2004, 86 sayfa

Terefitalik asit bis-(2-tiyofen-3-il-etil)ester (TATE), dekandioik asit bis-(2-tiyofen-3-il-etil) ester (DATE), oktanoik asit 2-tiyofen-3-il-etil ester (OTE) ve bunların homopolimerleri ve tiyofen ile kopolimerlerinin ve politiyofenin ısı ve yapısal özelliklerini araştırmak için piroliz kütle spektrometresi kullanılmıştır. Bütün örnekler için, çözücü ve reaksiyona girmemiş örneğin üstüne tutunmuş monomerin atılımı 100°C'nin altında gözlenmiştir. Sonuçlar, ester bağlarının arasında bulunan ara grubun etkileri göz önüne alınarak detaylı bir şekilde tartışılmıştır. Polimer ve monomerlerin ağırlık kaybını araştırmak için termal gravimetre analiz yöntemi kullanılmıştır. Örneklerin iletkenlikleri, dört- prob tekniği ile ölçülmüştür.

Ester bağları hidrokarbon zincirleri içerdiği zaman polimerin 2 ve 5 pozisyonlarından polimerleştiği gözlenmiştir. Diğer taraftan, ester grupları fenil gibi daha sıkı gruplara

sahip olduğunda sterik engellenmenin polimerizasyonun ikinci pozisyondan gerçekleşmesini engellediği, polimerizasyonun tiyofen grubu üstündeki 5 pozisyonundan ilerlediği ve oluşan polimerin daha düşük iletkenliğe sahip olduğu gözlenmiştir. P(OTE) için ağsal yapı P(DATE) ve P(TATE) den oldukça farklı olup PTh kıyasla oldukça düşüktür.

Kopolimer örneklerinde TATE, DATE veya OTE'nin varlığında ısı bozunum ürünlerinin çok fazla etkilenmediğini gösteren benzer ısı davranım karakterizasyonu gözlenmiştir.

Anahtar Kelimeler : elektropolimerizasyon, piroliz, politiyofen, ısı bozunum, kütle spektrometri

**TO MY FAMILY
WITH FULL COMPLIMENTS**

ACKNOWLEDGEMENTS

I would like to express my greatest appreciations to Prof. Dr. Jale Hacaloğlu and Prof. Dr. Levent Toppare and for their guidance, encouragements, patience and friendship throughout this work.

I would like to thank to, Dr. Ali Çırpan and Pınar Çamurlu for their help, technical support and answering my questions anytime in the laboratory, besides their kind friendship. I would like to thank all of my former and present lab mates for their kind friendship.

Appreciation is extended to colleagues in Department of Chemistry, Middle East Technical University.

Finally I would like to thank to my family for always being there for me.

TABLE OF CONTENTS

PLAGIARISM.....	iii
ABSTRACT.....	iv
ÖZ.....	vi
DEDICATION.....	viii
ACKNOWLEDGMENTS.....	ix
TABLE OF CONTENTS.....	x
LIST OF TABLES.....	xii
LIST OF FIGURES.....	xiii
LIST OF ABBREVIATIONS AND SYMBOLS.....	xvi

CHAPTER

I. INTRODUCTION.....	1
1.1 Conducting Polymers.....	1
1.1.1 Basic Principles	3
1.1.2 Electropolymerization	3
1.1.3 Doping Process.....	6
1.1.4 Conductivity and Electronic Structure of Conducting Polymers.....	7
1.1.5 Charge Carriers in Conducting Polymers.....	9
1.1.6 Hopping Process	11
1.1.7 Substituted Heterocycles	12
1.1.8 Electrochemical Polymerization in Lewis Acid	13
1.1.8 Degradation of Conducting Polymers.....	14

1.1.9 Applications	15
1.1.10 Characterization of Conducting Polymers.....	16
1.2 Mass spectrometry	16
1.2.1 Pyrolysis Mass Spectrometry	17
1.2.2 Direct Insertion Probe Pyrolysis Mass Spectrometry	18
1.3 Aim of the Study	19
 II. EXPERIMENTAL.....	 20
2.1. Materials	20
2.2 Instrumentation	20
2.2.1 Potentiostat	20
2.2.2. Electrolysis Cell.....	21
2.2.3 Thermal Gravimetry Analysis (TGA).....	21
2.2.4 Mass Spectrometer	21
2.2.4.1 Vacuum System.....	22
2.2.4.2 Sample Inlet	23
2.2.4.3 Ion Source.....	24
2.2.4.4 Mass Filter.....	25
2.2.4.5 Detector.....	26
2.2.5 Four Probe Conductivity Measurements	26
2.3 Procedure	28
2.3.1 Synthesis of Terephthalic acid bis-(2-thiophen-3-yl-ethyl)ester (TATE)	28
2.3.2 Electrochemistry of TATE.....	28
2.3.3 Synthesis of Decanedioic acid bis-(2-thiophen-3-yl-ethyl) ester (DATE)	29
2.3.4 Electrochemistry of DATE.....	29
2.3.5 Synthesis of Octanoic acid 2-thiophen-3-yl-ethyl ester (OTE)	30
2.3.6 Electrochemistry of OTE.....	30
 III. RESULTS AND DISCUSSION.....	 31
3.1 Polythiophene.....	32
3.2 DATE and Its Polymers	38

3.2.1 DATE	38
3.2.2 Homopolymer of DATE (P(DATE))	40
3.2.3 Copolymers of DATE with Thiophene	45
3.2.4 Thermal Gravimetric Analysis of DATE	51
3.2.5 Conductivity Measurements	51
3.2 TATE and Its Polymers	52
3.1.1. TATE	52
3.1.2 Homopolymer of TATE (P(TATE))	54
3.1.3 Copolymer of TATE with Thiophene	59
3.1.4 Thermal Gravimetric Analysis of TATE	65
3.1.5 Conductivities of TATE	65
3.3 OTE and Its Polymers	67
3.3.1 OTE	67
3.3.2 Homopolymer of OTE (P(OTE))	69
3.3.3 Copolymer of OTE with Thiophene (P(OTE-co-Th))	74
3.3.4 Thermal Gravimetric Analysis of OTE	80
3.3.5 Conductivity Measurements of OTE	80
IV. CONCLUSIONS	83
List of Publications	84
REFERENCES	85

LIST OF TABLES

TABLE

Table 1. Some polymers and their conductivity.....	13
Table 2 The characteristics and/or intense peaks present in the pyrolysis mass spectra corresponding to the maximum in the ion profiles recorded during the pyrolysis of PTh.	34
Table 3 The most and/or characteristic peaks of DATE and P(DATE) at some selected temperatures, with related chemical formula.....	42
Table 4 The most and/or characteristic peaks of P(DATE-co-Th) at some selected temperatures, with related chemical formula.....	50
Table 5 The most and/or characteristic peaks of TATE and P(TATE) at some selected temperatures, with related chemical formula.....	57
Table 6. The most and/or characteristic peaks of P(TATE-co-Th) at some selected temperatures, with related chemical formula.....	62
Table 7 The most and/or characteristic peaks of OTE and P(OTE) at some selected temperatures, with related chemical formula.....	71
Table 8 The most and/or characteristic peaks of P(OTE-co-Th) at some selected temperatures, with related chemical formula.....	79

LIST OF FIGURES

FIGURES

Figure 1.1 Some common conducting polymers	2
Figure 1.2 Electrochemical polymerization mechanism.....	5
Figure 1.3 Doping figure of anodic oxidative polymerization of thiophene.....	6
Figure 1.4 Schematic representation of band structure of a metal, a semiconductor and an insulator	8
Figure 1.5 Conductivity range	9
Figure 1.6 Schematic representations of solitons	10
Figure 1.7 Formation of polaron and bipolaron for polypyrrole	11
Figure 2.1 Block diagram of mass spectrometer.....	22
Figure 2.2 Direct Insertion Probe (DIP) Pyrolysis System.....	23
Figure 2.3 Path of Ramp Heating in Direct Insertion Probe.....	24
Figure 2.4 Schematic diagram of a quadrupole mass analyzer.....	26
Figure 2.5 Four probe conductivity measurements.....	27
Figure 3.1 TIC curve and mass spectra recorded at temperatures corresponding to the maximum ion yield for PTh.....	33
Figure 3.2 Single ion pyrograms of some selected fragments recorded during pyrolysis of PTh	36
Figure 3.3 Single ion pyrograms of monomer and the oligomers at m/z 84, 166, 248, 330, 412, 494 obtained during the pyrolysis of PTh.....	37
Figure 3.4 Mass spectra of DATE	38
Figure 3.5 a .The TIC curve and the mass spectra recorded at b. 80 ⁰ C, c. 170 ⁰ C,..... d. 230 ⁰ C, e. 265 ⁰ C and f. 440 ⁰ C	41
Figure 3.6 Single ion pyrograms of some selected fragments recorded during pyrolysis of P(DATE)	43

Figure 3.7 TIC curve recorded during the pyrolysis of a. P(DATE), b. P(Th), c. mechanical mixture corresponding homopolymers d. P(DATE-co-Th)	46
Figure 3.8 a .The TIC curve and the mass spectra recorded at b. 50 ⁰ C, c. 235 ⁰ C,..... d. 440 ⁰ C	47
Figure 3.8 The ion-temperature profiles of most intense and characteristic peaks as a function of temperature observed during pyrolysis of P(DATE-co-Th).....	49
Figure 3.9 TGA thermogram (a) DATE (b) P(DATE) (c)P(DATE-co-Th)	51
Figure 3.10 Mass spectra of TATE	52
Figure 3.11 a.The TIC curve and the mass spectra recorded at b. 75 ⁰ C, c. 200 ⁰ C, and..... d. 430 ⁰ C	56
Figure 3.12 The ion-temperature profiles of most intense and characteristic peaks as a function of temperature observed during pyrolysis of P(TATE)	58
Figure 3.13 TIC curve recorded during the pyrolysis of a. P(TATE), b. P(Th), c. mechanical mixture and d. P(TATE-co-Th).....	60
Figure 3.14 a. The TIC curve and the mass spectra recorded at b. 60 ⁰ C, c. 200 ⁰ C, and d.445 ⁰ C during the pyrolysis of P(TATE-co-Th)	61
Figure 3.15 Single ion pyrograms of some selected fragments recorded during pyrolysis of P(TATE-co-Th)	64
Figure 3.16.a TGA curve of TATE.....	65
Figure 3.16.b TGA thermogram of P(TATE).....	66
Figure 3.16.c TGA thermogram of P(TATE-co-Th).....	66
Figure 3.17 Mass Spectra of OTE.....	67
Figure 3.18 a. The TIC curve and the mass spectra recorded at b. 40 ⁰ C, c. 440 ⁰ C	70
Figure 3.19 The ion-temperature profiles of most intense and characteristic peaks as a function of temperature observed during pyrolysis of P(OTE)	73
Figure 3.20 TIC curve recorded during the pyrolysis of a. P(OTE), b. P(Th), c. mechanical mixture and d. P(OTE-co-Th)	75
Figure 3.21 a. The TIC curve and the mass spectra recorded at b. 35 ⁰ C, c. 60 ⁰ C, d. 425 ⁰ C.....	76
Figure 3.22 Single ion pyrograms of some selected fragments recorded during pyrolysis of P(OTE-co-Th).....	78
Figure 3.23 TGA thermogram of potentiostatically synthesized (a) P(OTE-co-Th) (b) P(Th) (c) P(OTE).....	80

LIST OF ABBREVIATIONS AND SYMBOLS

ABBREVIATIONS

ACN	Acetonitrile
BFEE	Boron trifluoro-diethyl etherate
CB	Conductance band
DATE	Decanedioic acid bis-(2-thiophen-3-yl- ethyl) ester
DCM	Dichloromethane
dc	Direct current
DIP-MS	Direct Insertion Probe Pyrolysis Mass Spectrometry
EI	Electron Impact
E_g	Band gap
HOMO	Highest occupied molecular orbital
LUMO	Lowest unoccupied molecular orbital
M^+	Molecular ion
MS	Mass spectroscopy
OTE	Octanoic acid 2-thiophen-3-yl-ethyl ester
PA	Polyacetylene
PPy	Polypyrrole
PTh	Polythiophene
Py	Pyrrole
Rf	Radio frequency
TATE	Terephthalic acid bis-(2-thiophen-3-yl-ethyl)ester
Th	Thiophene
TBABF	Tetrabutylammonium tetrafluoroborate
TEA	Triethyl amine
VB	Valence band

GREEK

α	1– position of the heterocycle
β	2– position of the heterocycle
π	pi-bonding orbital
π^*	pi-antibonding orbital

CHAPTER 1

INTRODUCTION

1.1 Conducting Polymers

Conducting polymer research has roots back to the 1960s where Pohl, Katon and others first synthesized and characterized semiconducting [1-3] and conjugated polymers [4]. The discovery of the high conductivity of poly(sulfurnitride) $(\text{SN})_x$, a polymeric inorganic explosive [5] and its interesting electrical properties [6,7] were a step towards conducting polymers as they are known today.

In 1862 Letheby reported the anodic oxidation of aniline in a solution of diluted sulfuric acid, and that the blue-black, shiny powder deposited on a platinum electrode was insoluble. After that, Goppelsroeder in 1876 suggested that anodically oxidized aniline had a chain-like, cyclic structure. In addition, this system could be electrochemically charged and discharged [8].

Conducting polymer research began when films of polyacetylene were found to exhibit profound increases in electrical conductivity when exposed to iodine vapor. The procedure for synthesizing polyacetylene was based upon a route discovered in 1974 by Shirikawa and coworkers through addition of 1000 times the normal amount of catalyst

during polymerization of acetylene [9]. The term “conducting polymers” was coined after the American scientists Heeger and MacDiarmid discovered the doping the “Shirakawa” polyacetylene with iodine in 1977 [10,11]. The successful doping of PA- in electrochemical terminology the equivalent of oxidation or reduction- encouraged the same scientists to test PA as a rechargeable active battery electrode [12]. Their promising results stimulated worldwide efforts to construct a polymer battery. In the course of these studies conducting polymers with similar to PA were discovered or rediscovered, such as polyparaphenylene, polypyrrole, polythiophene and, last but not least, polyaniline (Figure 1.1). However, it soon become apparent that the pathway from inspiration to practical realization can be long and thorny, that much basic research on a broad, interdisciplinary basis still has to be done [13].

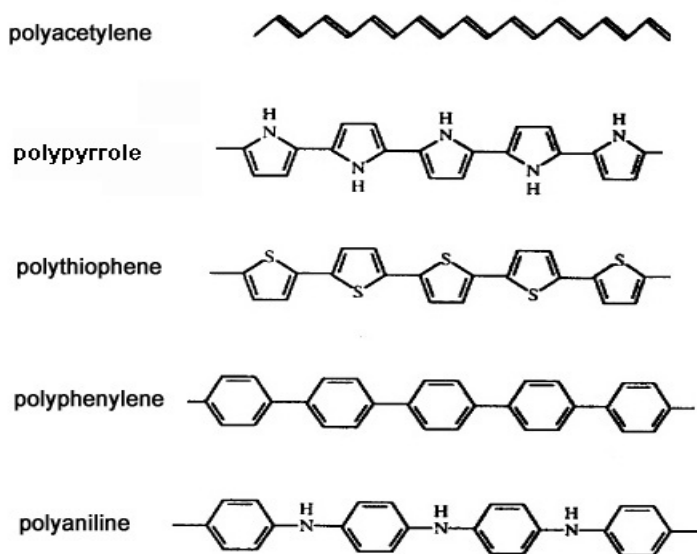


Figure 1.1 Some common conducting polymers

1.1.1 Basic Principles

Conducting polymers can be prepared via chemical or electrochemical polymerization [14]. The latter is generally preferred since it provides a better control of film thickness and morphology, and cleaner polymers when compared to chemical oxidation. Films of electronically conducting polymers are generally deposited onto a supporting electrode surface by anodic oxidation (electropolymerization) of the corresponding monomer species such as pyrrole [15], thiophene [16] or aniline [17] in the presence of an electrolyte solution.

Different electrochemical techniques can be used including potentiostatic (constant-potential), galvanostatic (constant-current) and potentiodynamic (potential scanning i.e. cyclic voltammetry) methods. Electrical conductivity is achieved in the film of conducting polymer by oxidation (p-doping) or reduction (n-doping), followed respectively by the insertion of anionic or cationic species. Due to the double bond alternation in the conjugated polymer backbone, the charged species formed upon doping are able to move along the carbon chain (delocalization) allowing electron transport and thus giving an electronically conductive material [18].

1.1.2 Electropolymerization

In an electrochemical polymerization, the monomer, dissolved in an appropriate solvent containing the desired anionic doping salt, is oxidized at the surface of an electrode by application of an anodic potential (oxidation). The choice of the solvent and electrolyte is of particular importance in electrochemistry since both solvent and electrolyte should be stable at the oxidation potential of the monomer and provide an ionically conductive medium [19]. Organic solvents like acetonitrile and propylene carbonate have very large potential windows, and high relative permittivities, which allow a good dissociation of

the electrolyte and thus a good ionic conductivity. As a result of the initial oxidation, the radical cation of the monomer is formed and reacts with other monomers present in the solution to form oligomeric products and then the polymer. The extended conjugation in the polymer results in a lowering of the oxidation potential compared to the monomer. Therefore, the synthesis and doping of the polymer are generally done simultaneously. The anion is incorporated into the polymer to ensure the electrical neutrality of the film and, at the end of the reaction; polymeric film of controllable thickness is formed at the anode. The anode can be made of a variety of materials including platinum, gold, glassy carbon, and tin or indium-tin oxide (ITO) coated glass. The electropolymerization is generally achieved by potentiostatic (constant potential) or galvanostatic (constant current) methods.

The electropolymerization mechanism is a controversial subject as there have been a number of mechanisms proposed to date. One of the principal difficulties encountered in the determination of the different stages of reaction is the rapidity of the polymerization. In addition, the insolubility of the polymers coupled with its non-crystalline nature makes structure characterization and analysis of physical properties exceedingly difficult. As a result, there has not been unanimous agreement among researchers concerning this mechanism.

The mechanism described by Diaz and his colleagues [20] is the mechanism encountered most often in the literature. Waltman and Bargon [21] have confirmed this mechanism by theoretical studies based on the correlation between the reactivity and the unpaired electron density of the radical cations.

This mechanism begins by electron transfer (E) followed by a succession of chemical reactions (C) and electron transfer reactions. The term $E(CE)_n$ which is an extension of the term ECE is often used to describe all the reactions involved in the formation of the film. This mechanism can be illustrated as shown in Figure 1.2 and the pathway is as the following:

(1) Oxidation of the monomer to a radical cation by loss of electron from the monomer. The oxidation of the thiophene is irreversible which shows that the cation radical formed in the first step is extremely reactive. (2) Coupling of two radicals to produce a dihydro dimer dication and rearomatization. This rearomatization constitutes the driving force of the chemical step. (3) Proton loss occurs to yield a neutral dimer and rearomatization. (4) Oxidation of the dimer to its radical cation. Due to the applied potential, the dimer, which is more easily oxidized than the monomer, occurs in its radical form. (5) Reaction of the dimer radical cation with another radical cation. (6) Electrochemical polymerization proceeds then through successive electrochemical and chemical steps until the oligomer becomes insoluble in the electrolytic medium and precipitates onto the electrode surface. The electrochemically prepared polymer film is already doped and contains the counterion.

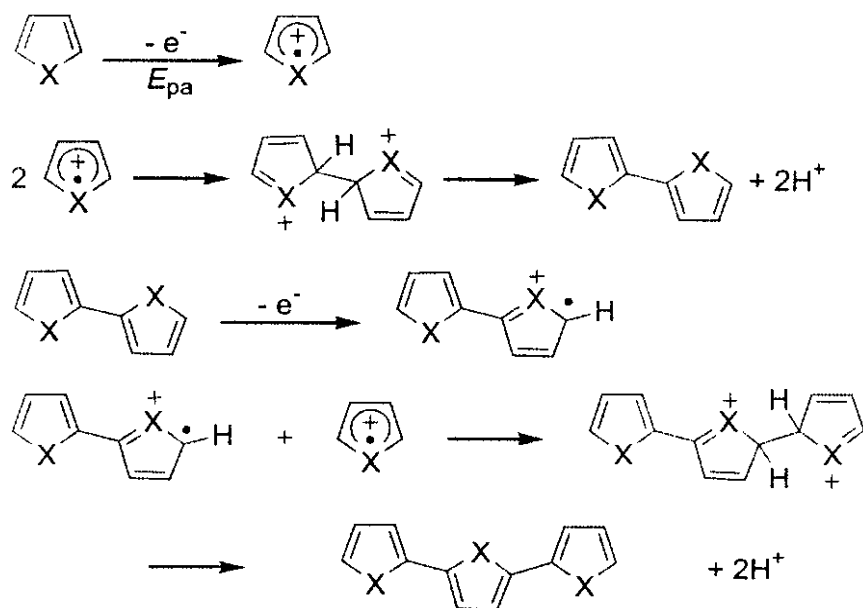


Figure 1.2 Electrochemical polymerization mechanism

1.1.3 Doping Process

A central point of electrochemical research is the analysis of doping mechanism. In the electrochemical terminology the doping process (Figure 1.3) corresponds to a redox reaction.

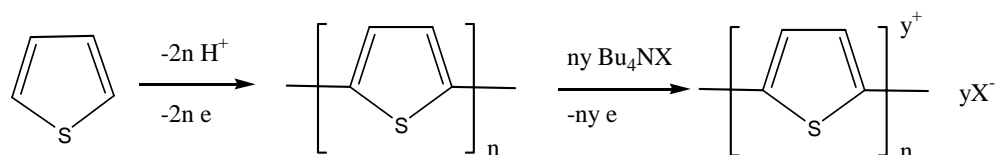


Figure 1.3 Doping figure of anodic oxidative polymerization of thiophene

Anions, termed ‘dopants’, are incorporated into the film to maintain electroneutrality. The doping terminology of conducting polymers should be distinguished from its conventional use in semi-conductor physics, since considerably higher concentration of dopant is employed in the former, typically up to 33% [22]. Conducting polymers can be cycled between the oxidized conducting state and the neutral insulating state, this process being controlled by the diffusion of counter ions into and out of the film [20].

Due to the relatively large band gaps in conjugated polymers, the concentration of charge carriers at low temperatures is very low. The doping of conducting polymers generates high conductivities primarily by increasing the carrier concentration [23]. Doping is reversible to produce the original polymer with little or no degradation of the polymer backbone. Both doping and undoping processes, involving dopant counterions which stabilize the doped state, may be carried out chemically or electrochemically. By controllably adjusting the doping level, conductivity anywhere between that of the non-doped (insulating or semiconductor) and that of the fully doped (conducting) form of the polymer is easily obtained. In the doped state, the backbone of a conducting polymer consists of a delocalized π system. In the undoped state, the polymer may have

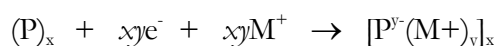
a conjugated backbone which is retained in a modified form after doping, or it may have a non-conjugated backbone which becomes truly conjugated only after p-doping [24].

p-Doping is the partial oxidation of the π backbone of an organic polymer. The basic process involves removing electrons to form a positively charged repeat unit



where P presents the basic monomeric repeat unit in the polymer.

Furthermore, if the polymer chain is partially reduced, the process is n type doping



1.1.4 Conductivity and Electronic Structure of Conducting Polymers

The electrical conductivities of materials allow them to be classified into three groups called conductors, semiconductors and insulators (Figure 1.4). In polymeric materials conduction may occur through the movement of either electrons or ions. In both cases electrical conductivity depends on a number of fundamental parameters, such as the number density of mobile charge carriers n , the charge q , and the carrier mobility μ . The relationship between conductivity σ and three latter quantities is expressed by the general relationship; $\sigma = n q \mu$.

The conduction mechanism can be explained by using the band theory. The atoms' outermost shells that contain the valence electrons are said to be in the valence band (VB). In order to provide conduction, an electron must gain sufficient energy to promote itself to the conduction band (CB). The energy difference between the valence and the conduction band is known as the band gap, E_g the size of which determines whether a material is an insulator, semiconductor or a conductor. In a semiconductor, band gap, E_g is narrow and the movement of electrons from the valence band to the

conduction band provides the conduction. In conductive materials, the highest energy level of the valence band and the lowest energy level of the conduction band are of similar energy that means there is no forbidden gap and electrons can easily pass from the valence band to the conduction band. The high conductivity of metals comes from partially occupied valence band or a zero band gap [25].

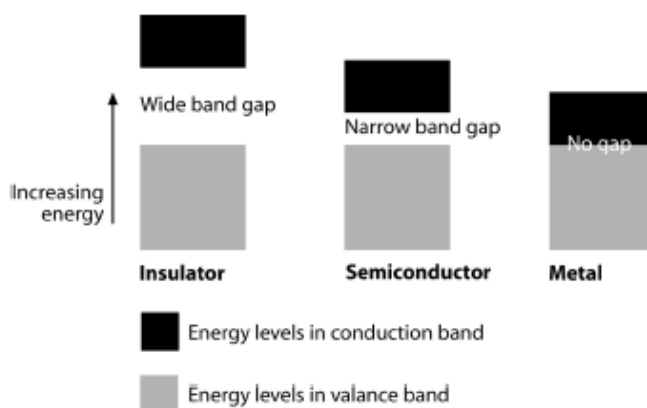


Figure 1.4 Schematic representation of band structure of a metal, a semiconductor and an insulator

In a semiconductor, band gap, E_g is narrow and the thermal excitation of electrons from the valence band to the conduction band provides the conduction. Otherwise in an insulator, the band gap E_g is too wide and the electrons cannot be excited thermally at room temperature from the valence band to the conduction band. Figure 1.5 shows the energy diagram for metals, semiconductors and insulators.

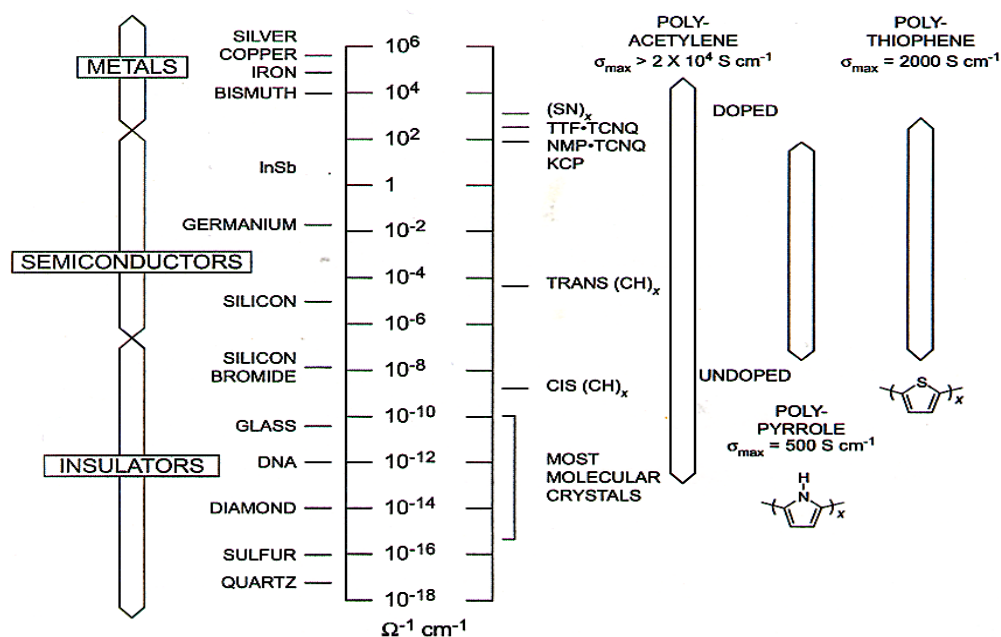


Figure 1.5 Conductivity range

1.1.5 Charge Carriers in Conducting Polymers

Mechanism for the electronic conductivity and the nature of charge carriers in conjugated polymers are still a subject of debate. A brief summary of the various theoretical models for the electronic conductivity of the conjugated polymers, using polyacetylene as an example, is given below (Figure 1.6).

The degeneracy of the ground state of polyacetylene produces structural defects in polymer chains, causing a change in bond alternation. At the defect side, a single unpaired electron exists, although the overall charge remains zero, creating a new energy level at mid-gap (a non-bonding orbital). This neutral defect state, known as a 'soliton', is singly occupied, possessing a spin of $\frac{1}{2}$, and is delocalized over about fifteen carbon atoms [26].

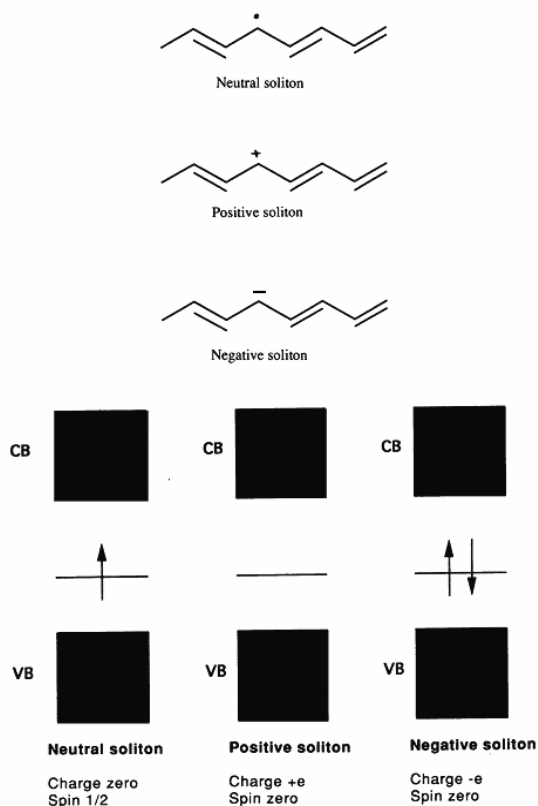


Figure 1.6 Schematic representations of solitons

The soliton energy levels can accommodate zero, one or two electrons and thus the soliton may also be positively or negatively charged, giving the unusual property of separating spin and charge, with neutral solitons possessing spin, but no charge, and charged solitons having no spin. In doped polymer, charge is localized in the mid-gap states, since these provide the HOMO for charge removal and the LUMO for charge injection. Since a defect can occur anywhere along the chain, there is translational symmetry in the system, providing mobility of the soliton along the chain, offering a mechanism for electronic conductivity.

Two neutral solitons usually recombine eliminating structural defects although single solitons can arise on chains with imperfections [27, 28]. In contrast, charged solitons repel each other and lead to isolated charged defects [26]. A neutral soliton and a charged one can however achieve a minimum energy configuration by pairing, producing a ‘polaron’ [29], which is essentially a radical cation, and gives rise to two states in the band gap, a bonding and an anti-bonding orbital, with symmetry placed about the mid-gap energy (Figure 1.7).

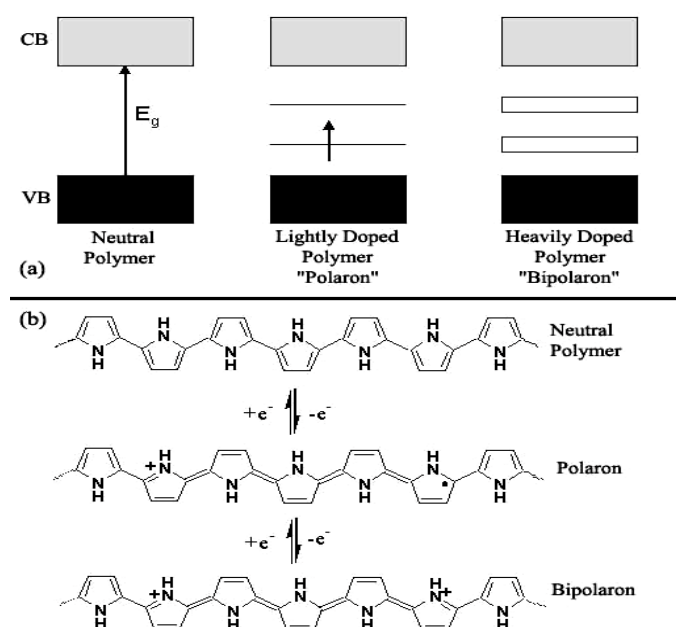


Figure 1.7 Formation of polaron and bipolaron for polypyrrole

1.1.6 Hopping Process

Although discussed charge carriers are responsible for electrical conductivity in conjugated polymers, many structural imperfection are present in all polymers and thus when discussing mechanism of bulk conductivity, these defects need to be considered. Conductivity is not only a result of charge transfer along the chain, but is also due to

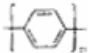
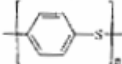
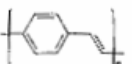
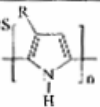
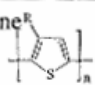
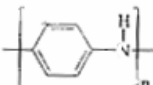
electron hopping between chains and between different conjugated segments of the same chain. In addition to these effects which act at a molecular level, bulk conductivity values are also dominated by electron transfer between grain boundaries and variation in morphology [30, 31].

1.1.7 Substituted Heterocycles

Pyrrole and thiophene substituted at the 3-(β -) position (and also the N-position for pyrrole) can often undergo electropolymerization to produce conducting polymers, since the 2- and 5-(α -) positions remain available for monomer coupling. The electrochemical behavior of a wide-range of β -substituted pyrroles and thiophenes has been investigated, although β -substituted thiophenes are generally more suitable than their pyrrole analogues due to their high stability and easy preparation [32]. The products formed from electro-oxidation are highly dependent on the substituent, with some reactions producing conducting polymers and others, insulating layers or soluble species. This has been attributed to electronic and steric factors.

Thus, in principle, a substituent may be chosen to produce the desired electrochemical properties. In addition to electronic effects, steric factors also influence the electrochemical polymerization and properties of conducting polymers, where they are formed [33]. Table 1 lists some of these polymers along with their electrical conductivity.

Table 1. Some polymers and their conductivity

Polymer	$\sigma / \Omega^{-1}\text{cm}^{-1}$	Stability (doped state)	Processing possibilities
Polyacetylene -HC=CH-	$10^3\text{-}10^5$	POOR	Limited
Polyphenylene 	1000	POOR	Limited
PPS 	100	POOR	Excellent
PPV 	1000	POOR	Limited
Polypyrroles 	100	GOOD	GOOD
Polythiophene 	100	GOOD	Excellent
Polyaniline 	10	GOOD	GOOD

1.1.8 Electrochemical Polymerization in Lewis Acid

Intensive efforts in the area of the electrochemical synthesis of conducting polymers are to optimize the preparation by controlling the system and parameters. Boron flouride-ethyl ether (BFEE) is a promising system which has been used for electrochemical synthesis of some heterocyclics like thiophene, pyrrole and bithiophene. Electrochemical polymerization of thiophene in BFEE yields a free standing film with good mechanical properties [34]. High applied potentials support the degradation of the polymer and side reactions of the electrolytes and electrodes [35]. BFEE lowers the

aromatic resonance energy and promotes the abstraction of an electron from the α -position of the heterocyclic ring, hence, assists the electrochemical polymerization. It is known that BFEE exists in diethyl ether as a polar adduct and the presence of a small amount of water results in the formation of $\text{H}^+[(\text{BF}_3\text{OH})]^-$, which affords a conducting medium, where the $[(\text{BF}_3\text{OH})]^-$ anion serves as the dopant throughout the polymerization.

1.1.8 Degradation of Conducting Polymers

Functional properties of polymers can be lost by degradation processes involving chemical reactions. The presence of reactive sides in the polymer and some external factors such as heat, oxygen, moisture and light may degrade polymer.

The instability of the conducting polymers may be caused by extrinsic degradation in which polymer chain reacts with oxygen, moisture, solvent and supporting salt. The instability of the conducting polymers may also be caused by intrinsic degradations, which can alter some chemical reactions, and consequently some changes in the structure of conducting polymers. Intrinsic degradation is affected by the reactivity of the dopant and the polymer backbone [36,37]. Therefore, p-type doped polymers prone to the degradations even when they are pure.

Reactions of the main chain with its counterion lead to irreversible loss of conjugation and electrical conductivity. For example, the dopants such as ClO_4^- with strong oxidizing ability cause conductivity decay in the polymer.

Atmospheric moisture may be considered as another potential external degradant for conducting polymers. The process may include electronic interaction of water with polymer carbonium ion or heteroatom, charge transfer, proton abstraction from the polymer chain or from water, hydroxylation of the polymer chain, protonation of the counterion and removal of the products of the compensation reaction. The depletion of counterion content consequently causes the loss of electrical conductivity. The

reversibility of the electrical conductivity on redoping may be predicted in this process. Atmospheric moisture leads degradation but conductivity can be gained by redoping.

Oxygen promotes degradation during electrooxidation and the physical properties. Reaction of the main chain with oxygen, leads to irreversible loss of conjugation and electrical conductivity. Ionization potential plays an important role in oxidative degradation of polymers. It should be high enough to protect polymer from transfer of an electron to oxygen to form a stabilized ion pair.

One of the parameters affecting the stability of the polymer is the chemical reactivity of the material itself. It is composed of linear chains with an alternation of single and double bonds. Chemical reactions of O_2 with a double bond can easily occur which break the π electron delocalization and the chemical structure. Thus electrical properties are then greatly affected. The degraded films have shorter π -conjugation lengths and are no longer dopable as a result.

1.1.9 Applications

There is a quite a large number of feasible technical applications of conducting polymers. The most advanced developments concern the rechargeable polymer battery [38-40]. Its attraction lies in the low weight of polymers as well as in environmental benefits. For polypyrrole [39] and polyaniline [38] commercially available cells already exist or are in preparation.

Another electrochemical application of conducting polymers may be their use as electrochromic displays [40-43]. They are based on the fact that the color of a polymer changes during electrochemical charging and discharging. Thus, polyaniline appears, to be particularly promising, as its colors changes during oxidation from yellow, through green, to blue and violet, and this process is reversed during discharging.

The optical properties of conducting polymers in the doped state can also be used for the preparation of antistatic, almost transparent materials [44]. Such a system is polymethoxydithiophene, which absorbs in the doped state in the near IR.

In recent years further concepts have been developed for the practical use of conducting polymers. They involve polymer based diodes and transistors [45], chemical sensors [46] or memory devices [47].

1.1.10 Characterization of Conducting Polymers

The main problem in characterization of the electrically conductive polymers comes from the property that gives it, its conductivity, and the conjugated backbone. Usually, conducting polymers exist in the form of insoluble and nonprocessable films, which prevents its analysis by conventional analytical methods. Characterization methods are therefore restricted to surface techniques and the following methods have been used with varying degrees of success: (i) electrochemical methods, particularly cyclic voltammetry (CV), (ii) X-ray photoelectron spectroscopy (XPS), (iii) solid- state NMR, typically ^{13}C NMR using cross polarization magic angle spinning (CPMAS ^{13}C NMR), (iv) scanning electron microscopy (SEM), and (v) scanning probe microscopy (SPM). Yet, little is known about the molecular, structural, physical properties and degradation behavior of conducting polymers. Recently, it has been shown that a more detailed characterization of conducting polymers can be achieved by the application of mass spectrometry [48,49].

1.2 Mass spectrometry

Mass spectrometry (MS) is an analytical technique in which atoms or molecules from a sample are ionized (usually positively), separated according to their *mass-to-charge* (m/z), and then recorded. The instrument used to carry out this measurement is called a mass spectrometer.

Mass Spectrometry (MS) is an analytical spectroscopic tool primarily concerned with the separation of molecular (and atomic) species according to their mass. MS can be used in the analysis of many types of sample from elemental to large proteins and polymers

Mass spectrometry had its birth in 1886 when Goldstein, a German physicist, discovered positive ions in a low-pressure electrical discharge tube. In 1898, Wien showed that a beam of these ions could be deflected by using electric and magnetic fields. Between 1912 and 1919, Thompson and Aston managed to resolve ion trajectories corresponding to mass differences of less than 10%, thus enabling them to confirm the existence of two distinct neon isotopes. In 1922, Aston received the Nobel Prize for his work and by 1924 he had characterized the isotopic abundances of around fifty elements. Reliable mass spectrometers, for use in the petroleum industry, became available in the early 1940s [50].

1.2.1 Pyrolysis Mass Spectrometry

Pyrolysis mass spectrometry is a very sensitive technique applied for structural characterization of inorganic, organic and bioorganic compounds. Molecules have distinctive fragmentation patterns that provide structural information to identify structural components. Pyrolysis mass spectrometry can be utilized for investigation thermal stability, thermal degradation mechanisms and decomposition products of polymers. It can also be used to study the stereoregularity of the homopolymers through tetramers or higher oligomers.

Pyrolysis is the thermal degradation of a material in an inert atmosphere or in vacuum. It causes molecules to cleave at their weakest points to produce smaller, volatile fragments called pyrolysate [51]. Pyrolysis products can be identified by mass spectrometry (MS), gas chromatography (GC) and infrared spectroscopy (IR)

Among the various pyrolysis mass spectrometry techniques direct pyrolysis mass spectrometry technique allows the thermal decomposition products of the polymer

sample to be observed directly in the ion source of the mass spectrometer, so that the evolving products are ionized and continuously detected by repetitive mass scans almost simultaneously with their formation. Since pyrolysis is accomplished under high vacuum, the thermal degradation fragments are removed from the hot zone, thus molecular collisions have low probability the generation of secondary reactions is reduced [52]. It is a simple and quick method for structural and thermal characterization of polymers [53,54].

1.2.2 Direct Insertion Probe Pyrolysis Mass Spectrometry (DIP-MS)

The direct pyrolysis technique has been used for obtaining the structural information of high molecular weight chemicals. Mass spectrometry only separates and detects gas phase ions. Usually, ionization occurs in the gas phase. Therefore, a sample that is a solid, liquid or part of a solution should be converted into the gas phase before subjecting analysis by mass spectrometry. For solids, sample volatilization is achieved by using a Direct Insertion Probe. It has the advantages of allowing a simple and a quick analysis with a small amount of sample for structural and thermal characterization of the polymers.

In direct insertion probe pyrolysis mass spectrometry technique; pyrolysis is carried out inside the mass spectrometer under high vacuum conditions of the MS. Thus, besides the low molecular weight products, relatively high molecular weight and unstable fragments can also be analyzed since condensation is prevented. The collision of fragments and the possibility of secondary reactions are minimized by means of high vacuum conditions and mainly primary degradation products are detected. Furthermore, unstable thermal degradation products can also be monitored during the pyrolysis. The temperature is increased gradually and the degradation products as a function of temperature can be detected continuously during the process.

1.3 Aim of the Study

The objectives of this study are:

- To achieve the electrochemical polymerization of terephthalic acid bis-(2-thiophen-3-yl-ethyl)ester (TATE), decanedioic acid bis-(2-thiophen-3-yl-ethyl) ester (DATE), octanoic acid 2-thiophen-3-yl-ethyl ester (OTE)
- To achieve electrochemical polymerization of TATE, DATE, OTE in the presence of thiophene to obtain the conducting copolymers
- To determine thermal behavior, decomposition products and degradation mechanism of BF_4^- doped P(TATE), P(DATE), P(OTE) and polythiophene
- To investigate the effects of each component of the polymer on structural and thermal characteristics
- To determine the effect of substituent group on thiophene ring via pyrolysis methods

CHAPTER 2

EXPERIMENTAL

2.1. Materials

2-Thiophen-3-yl-ethanol (Aldrich), terephthaloyl chloride (Aldrich), sebacoylchloride (Aldrich), octanoyl chloride (Aldrich), triethylamine (TEA) (Merck), dichloromethane (DM) (Merck), methanol (Merck), acetonitrile (AN) and borontrifluoride ethylether (Aldrich) were used without further purification. Thiophene (Aldrich) was distilled before use. Tetrabutylammonium tetrafluoroborate (TBAFB) (Aldrich) was used as received.

2.2 Instrumentation

2.2.1 Potentiostat

A Wenking POS 73 potentiostat was used to provide the constant potential in electrochemical syntheses. Potentiostat keeps the voltage difference between working electrode and reference electrode at a constant value despite the changes in the current passing through the electrolytic cell, the concentration of the electroactive substance, and the solution resistance. The current supplied by the potentiostat can be determined by measuring the voltage drop across a resistance connected to the counter electrode in series. To compensate the changes in potential of working electrode, potentiostat

continuously checks the potential of working electrode measured with respect to reference electrode, and changes the potential difference in between to maintain the desired potential value that was set.

2.2.2. Electrolysis Cell

Polymerization reactions were carried out in a one-compartment cell with three-electrode configuration. Platinum (Pt) flag electrodes (1.5 cm^2) as the working and counter and silver (Ag) wire (pseudo reference) reference electrode were used during electrolyses, and all potentials were reported with respect to the Ag wire. The cell has gas inlets to pass the N_2 gas through the solution in order to achieve inert medium and to prevent the oxidation during the electrolysis.

2.2.3 Thermal Gravimetry Analysis (TGA)

Du Pont 2000 Thermal Gravimetry Analyzer was used to investigate the thermal behavior of polymers and monomers; weight loss was followed upon heating. TGA experiments were performed by heating rate of $10\text{ }^\circ\text{C}/\text{min}$ under N_2 atmosphere.

2.2.4 Mass Spectrometer

Direct insertion probe pyrolysis mass spectrometry (DIP-MS) system consists of a 5973 HP quadrupole mass spectrometer coupled to a JHP SIS direct insertion probe. This system provides fast scanning; self-tuning of experimental parameters and wide mass range. Mass spectra of the products were recorded at a scan rate of 2 scan/s in the mass range of $10\text{-}800\text{ amu}$.

The major components of mass spectrometer are vacuum system, sample inlet, ion source, mass filter, detector and the data system (Figure 2.1).

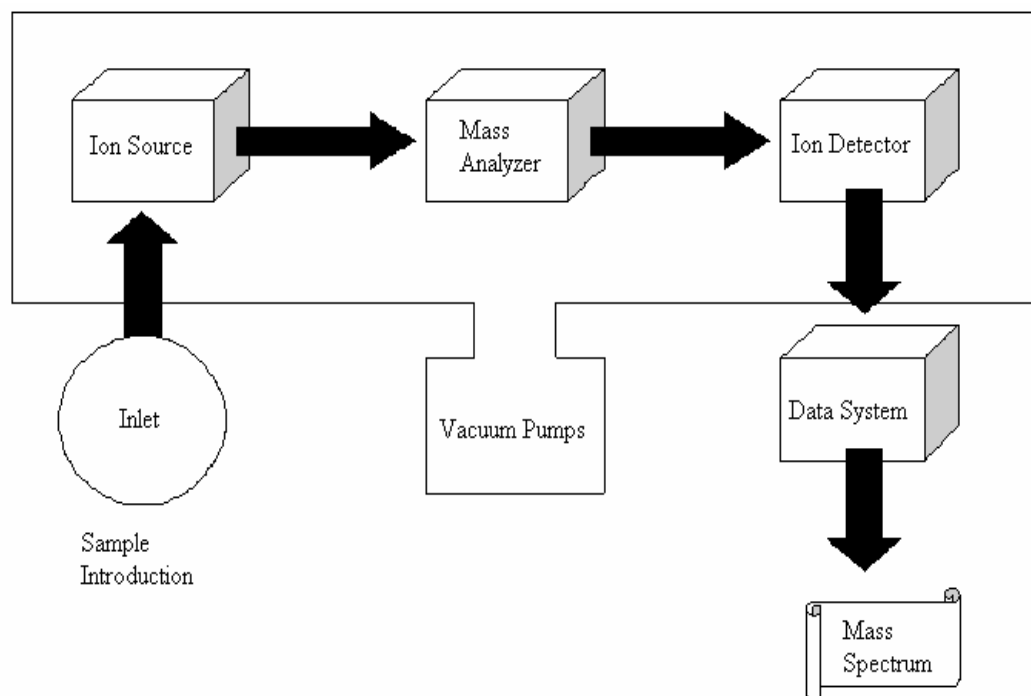


Figure 2.1 Block diagram of mass spectrometer

2.2.4.1 Vacuum System

The vacuum system creates the high vacuum (low pressure) required for the mass spectrometer to operate so that it makes it possible for ions generated by electron impact in the ion source to move from the ion source to the quadrupole analyzer where they are separated according to their mass to charge (m/z) ratios and then to the detector without collisions with other ions and molecules. A high vacuum is obtained by diffusion and rotary vane pumps.

2.2.4.2 Sample Inlet

The Direct Insertion Probe Pyrolysis technique is employed by a SIS direct inlet probe (Figure 2.2). The heating rate can be controlled by a thermocouple attached to the probe tip inside the probe rod and the probe tip is in direct contact with flared glass sample vials that can be inserted and removed from the direct probe inlet easily.

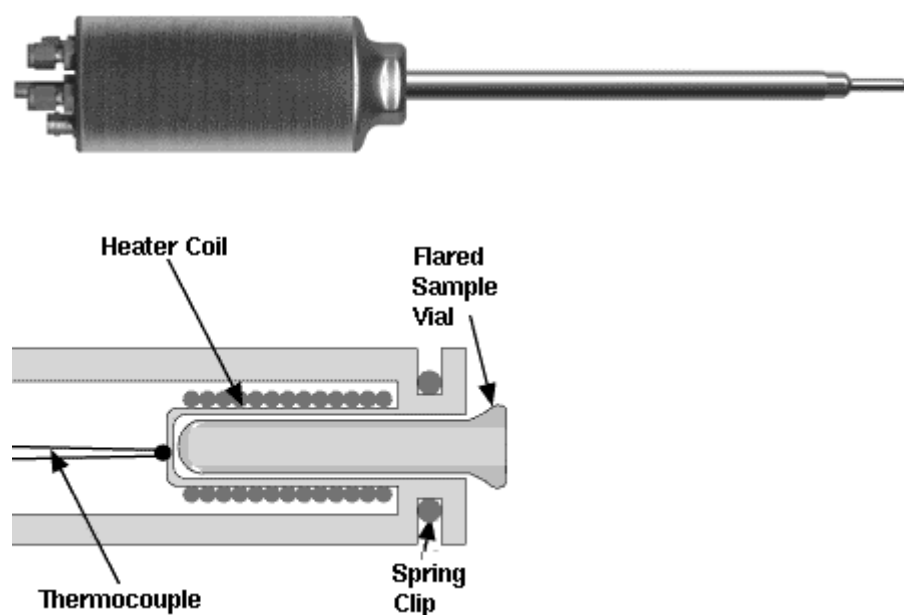


Figure 2.2 Direct Insertion Probe (DIP) Pyrolysis Sytem

The heating rates are programmed with the use of the probe software. Generally, ramping heating is applied. Direct pyrolysis experiments were performed by applying a program which allows a heating rate of $10^{\circ}\text{C}/\text{min}$ (Figure 2.3). In each experiment, the temperature was increased up to 445°C , (the maximum attainable temperature) and kept constant for an additional 10 minutes at 445°C . Each set of analysis involves 5400 mass spectra.

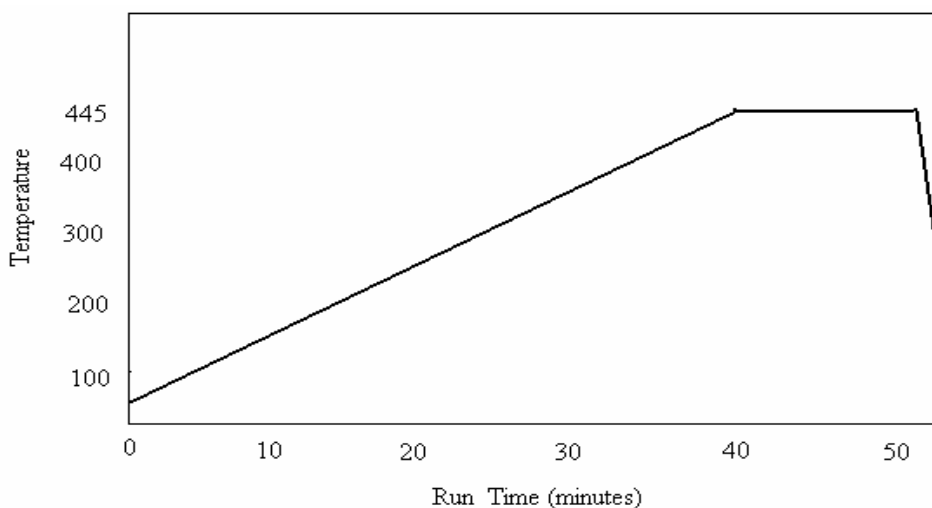


Figure 2.3 Path of Ramp Heating in Direct Insertion Probe

2.2.4.3 Ion Source

Sample molecules enter the ion source from the sample inlet. Before the ion source, the sample molecules must be converted into the pyrolyzed form. In the ion source, ionization and the fragmentation of the molecules are occurred.

The ion source operates by electron impact ionization (EI). Electrons are produced by thermionic emission from a tungsten or rhenium filament. A typical filament current is 1×10^{-4} Amps. These electrons leave the filament surface and are accelerated towards the

ion source chamber which is held at a positive potential (equal to the accelerating voltage). The electrons acquire energy equal to the voltage between the filament and the source chamber - typically 70 electron volts (70 eV). The electron trap is held at a fixed positive potential with respect to the source chamber. A proportion of the electron beam will strike the electron trap producing the trap current. This is used as a feedback circuit to stabilize the electron.

The positive ion repeller voltage and the negative excitation voltage work together to produce an electric field in the source chamber such that ions will leave the source through the ion exit slit. The ions are directed through the various focusing and centering lenses and are focused onto the source exit slit. The ions can then be mass analyzed.

2.2.4.4 Mass Filter

The mass filter separates ions according to their mass to charge ratio (m/z). At a given time, only ions of a selected mass to charge ratio can pass through the filter to the detector. The analyzer is a quadrupole mass filter (Figure 2.4).

In a quadrupole mass analyzer, only electric fields are used to separate ions according to their m/z values. A quadrupole consists of four parallel rods or poles through which the ions being separated are passed. The poles have a fixed DC and alternating RF voltages applied to them. Depending on the produced electric field, only ions of a particular m/z will be focused on the detector, all the other ions will be deflected into the rods. By varying the strengths and frequencies of electric fields, different ions will be detected thus making the mass spectrum.

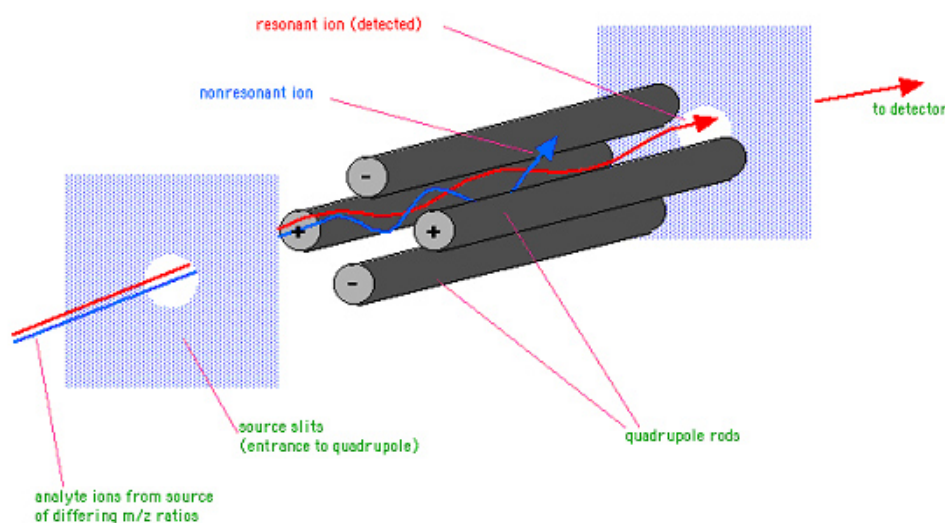


Figure 2.4 Schematic diagram of a quadrupole mass analyzer

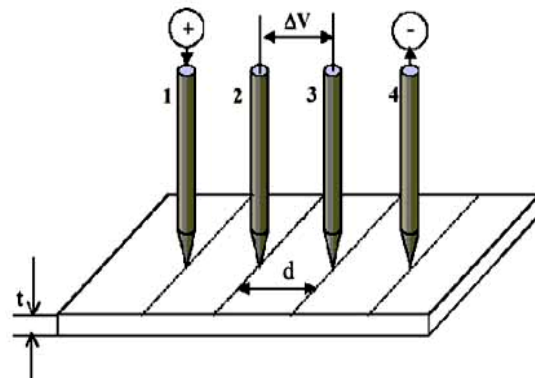
2.2.4.5 Detector

The detector in the spectrometer is a high-energy conversion dynode (HED) coupled to an electron multiplier (EM). The detector is located at the exit end of the quadrupole mass filter. It receives the ions that have passed through the mass filter.

2.2.5 Four Probe Conductivity Measurements

Among available conductivity techniques, four-probe method is more advantageous for measuring electrical properties of conducting polymers. This technique eliminates errors caused by contact resistance, since the two contacts measuring the voltage drop are different from the contacts applying the current across the sample.

Figure 2.5 shows the simplest form of a four-point probe measurement setup. A row of pointed electrodes touches the surface of a polymer film taped or spin cast on an insulating substrate. A known current I is injected at the electrode 1 and is collected at the electrode 4, while the potential difference ΔV between contacts 2 and 3 is measured. Conductivity is calculated from the following equation:



$$\sigma = \ln 2 / (\pi d \times R)$$

σ : Conductivity

R : the resistance of the sample

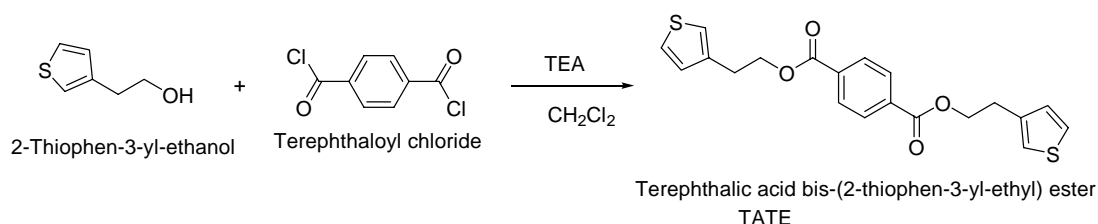
d : sample thickness.

Figure 2.5 Four probe conductivity measurements

2.3 Procedure

2.3.1 Synthesis of terephthalic acid bis-(2-thiophen-3-yl-ethyl)ester (TATE)

2-Thiophen-3-yl-ethanol (1.12 mL, 0.001 mol) was dissolved in 10 mL dichloromethane containing 1.11 mL (0.008 mol) triethylamine (TEA). To this solution 0.81 g terephthaloyl chloride (0.004 mol) in 10 mL of dichloromethane were added dropwise in 0.5 h, by cooling in ice bath and nitrogen atmosphere. The esterification was carried out for overnight at 0 °C. Then the solution was washed with HCl 1% solution (three times) and water (three times). The organic layer was dried over Na₂SO₄ and the solvent was removed via rotaevaporatory. Twice recrystallization from ethanol provided 1.1 g of white crystals (yield 71%) [55]. Route for synthesis is shown in scheme (1)



Scheme 1. Synthesis route for TATE

2.3.2 Electrochemistry of TATE

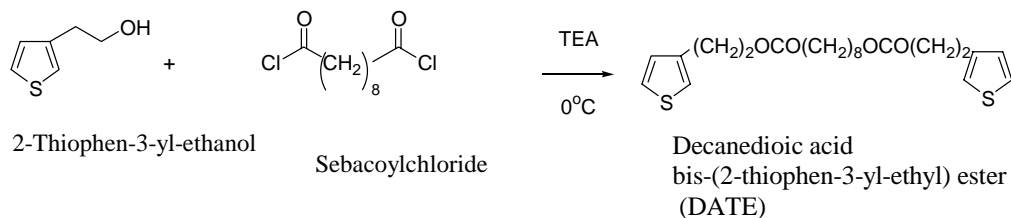
Homopolymerization of TATE was achieved via constant potential electrolysis by Wenking POS 73 potentiostat in a one-compartment cell. 0.01 M TATE dissolved DM/BFEE (8:2, v/v). 0.1 M TBAFB used as the supporting electrolyte and electrolysis performed at 1.6 V. Working and counter electrodes were Pt and reference electrode was Ag/Ag⁺. For the copolymerization of TATE with thiophene, constant potential electrolysis was carried out in DM/BFEE (8:2, v/v) solution composed of 0.01 M TATE, 0.1 M TBAFB, 15μL thiophene at 1.6 V in a one compartment cell where the

working and counter electrodes were Pt and reference electrode was Ag/Ag⁺. Films were washed several times to remove the unreacted monomer and TBAFB.

2.3.3 Synthesis of decanedioic acid bis-(2-thiophen-3-yl- ethyl) ester (DATE)

2-Thiophen-3-yl-ethanol (1.1mL, 1mmol) was dissolved in 10 mL dichloromethane containing (0.07 mL, 0.5 mmol) triethylamine (TEA). To this solution sebacoylchloride (0.1mL, 0.5 mmol) was added dropwise in 0.5 h, by cooling in ice bath and nitrogen atmosphere. The solution was washed with HCl 1% solution and water. The organic layer was dried over MgSO₄ and the solvent was removed via rotary evaporator. DATE was obtained as a light yellowish solid (0.184g, 0.436mmol, 87%) mp 73^oC [56]. Route for synthesis is shown in scheme (2)

The representation of synthesis is demonstrated in Scheme 2.



Scheme 2. Synthesis route for DATE

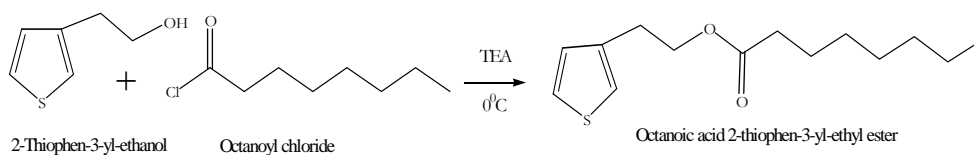
2.3.4 Electrochemistry of DATE

Preparative electrochemical homopolymerization was performed under potentiostatic conditions in a one-compartment cell. 0.01M DATE dissolved in ACN/BFEE (8:2, v/v) solvent mixture and 0.1 M TBAFB used as the supporting electrolyte. Electrolyses

were carried out at 1.5V equipped with Pt working and counter electrodes and Ag/Ag⁺ reference electrode at room temperature for 1h. Copolymerization was achieved under same conditions in the presence of 15 μ L of thiophene. The freestanding films were washed with ACN several times to remove unreacted monomer and TBAFB.

2.3.5 Synthesis of octanoic acid 2-thiophen-3-yl-ethyl ester (OTE)

Stoichiometric amount of 2-thiophene-3-yl ethanol, triethylamine (TEA) were dissolved in 20 mL dichloromethane. Octanoyl chloride was added drop wise to this mixture at 0⁰C under inert atmosphere. The resulting liquid monomer was purified with successive extractions and dried by anhydrous MgSO₄ [57]. Route for synthesis is shown in scheme (3)



Scheme 3. Synthesis route for OTE

2.3.6 Electrochemistry of OTE

The homopolymerization of OTE via constant potential electrolysis was performed in a single compartment cell, in the presence of 0.01M OTE, 0.1 M TBAFB in ACN/BFEE (8:2, v/v) by application of 1.5V, equipped with Pt working and counter electrodes and a Ag/Ag⁺ reference electrode for 1h. Copolymerization was achieved under same conditions in the presence of 15 μ L of thiophene. The freestanding films were washed with ACN several times to remove unreacted monomer and TBAFB.

CHAPTER 3

RESULTS AND DISCUSSION

In order to investigate the thermal and structural characteristics of terephthalic acid bis-(2-thiophen-3-yl-ethyl)ester (TATE), decanedioic acid bis-(2-thiophen-3-yl-ethyl) ester (DATE) and octanoic acid 2-thiophen-3-yl-ethyl ester (OTE), their corresponding homopolymers, copolymers with thiophene and polythiophene have been analyzed in terms of their pyrolytic behavior. Furthermore Thermal Gravimetry Analysis was performed to support pyrolysis data. Conductivity measurements have also been carried out to investigate effects of structure on conductivity.

By examining the tables and figures, one may notice that the multiplication factors in the figures and abundance ratios given in the tables do not match. The multiplication factors in the figures are determined comparing the pyrolograms (the time-temperature resolved ion-current curves); whereas the abundance ratios observed in the tables are related to the mass spectral data recorded at the temperature corresponding to maximum ion yield.

3.1 Polythiophene

The total ion current (TIC) curve for BF_4^- doped polythiophene is given in Figure 3.1. Three peaks with maxima at 60, 250 and 440°C can be seen in the TIC curve. The mass spectra recorded at these temperatures are also included in Figure 3.1. It is easily noticed that the mass spectra were quite complicated as expected due to the further dissociation of thermal degradation products during ionization in the mass spectrometer. In order to determine the effect of dissociative ionization, the pyrolysis experiments were repeated decreasing ionization energy from 70 eV to 19 eV. Both 70 and 19 eV TIC curves showed similar trends. Furthermore, both pyrolysis mass spectra were dominated with the same product peaks.

The pyrolysis mass spectra indicated that at initial stages of pyrolysis, at temperatures lower than 100°C, the evolution of the solvent, water, adsorbed dopant and its counter ion Bu_4N^+ occurred. Decomposition products of dopant started to appear in the pyrolysis mass spectra recorded above 100°C. Evolutions of dopant based products were observed in 120°C and 350°C. The most intense fragment is BF_2^+ ($m/z=49$ Da) and its maximum yield was observed at 250°C. Peaks that can be associated with thermal degradation of PTh were detected in the final stage of pyrolysis. Oligomer peaks up to six monomer units were present in the spectra. Moreover, in the final stage of pyrolysis, some peaks that can be associated with the degradation of thiophene (Th) ring such as peaks due to C_2H_2 ($m/z=26$ Da), S ($m/z=32$ Da), H_2S ($m/z=34$ Da), C_3H_3 ($m/z=39$ Da), HCS ($m/z=45$ Da), $\text{C}_3\text{H}_3\text{S}$ ($m/z=71$ Da), $(\text{C}_2\text{H}_2\text{S}_2)_2$ ($m/z=116$ Da), $\text{C}_4\text{H}_3\text{SCH}_2$ ($m/z=97$ Da), $\text{C}_4\text{H}_3\text{S}-\text{C}_4\text{H}_2\text{S}-\text{CH}_2$ ($m/z=179$ Da) and $\text{C}_4\text{H}_3\text{S}-(\text{C}_4\text{H}_2\text{S})_2-\text{C}_2\text{H}_2$ ($m/z=273$) were also recorded. The relative intensities of some of characteristics and/or intense peaks in the 70 and 19 eV mass spectra recorded at 250 and 440°C and their assignments are given in Table 2.

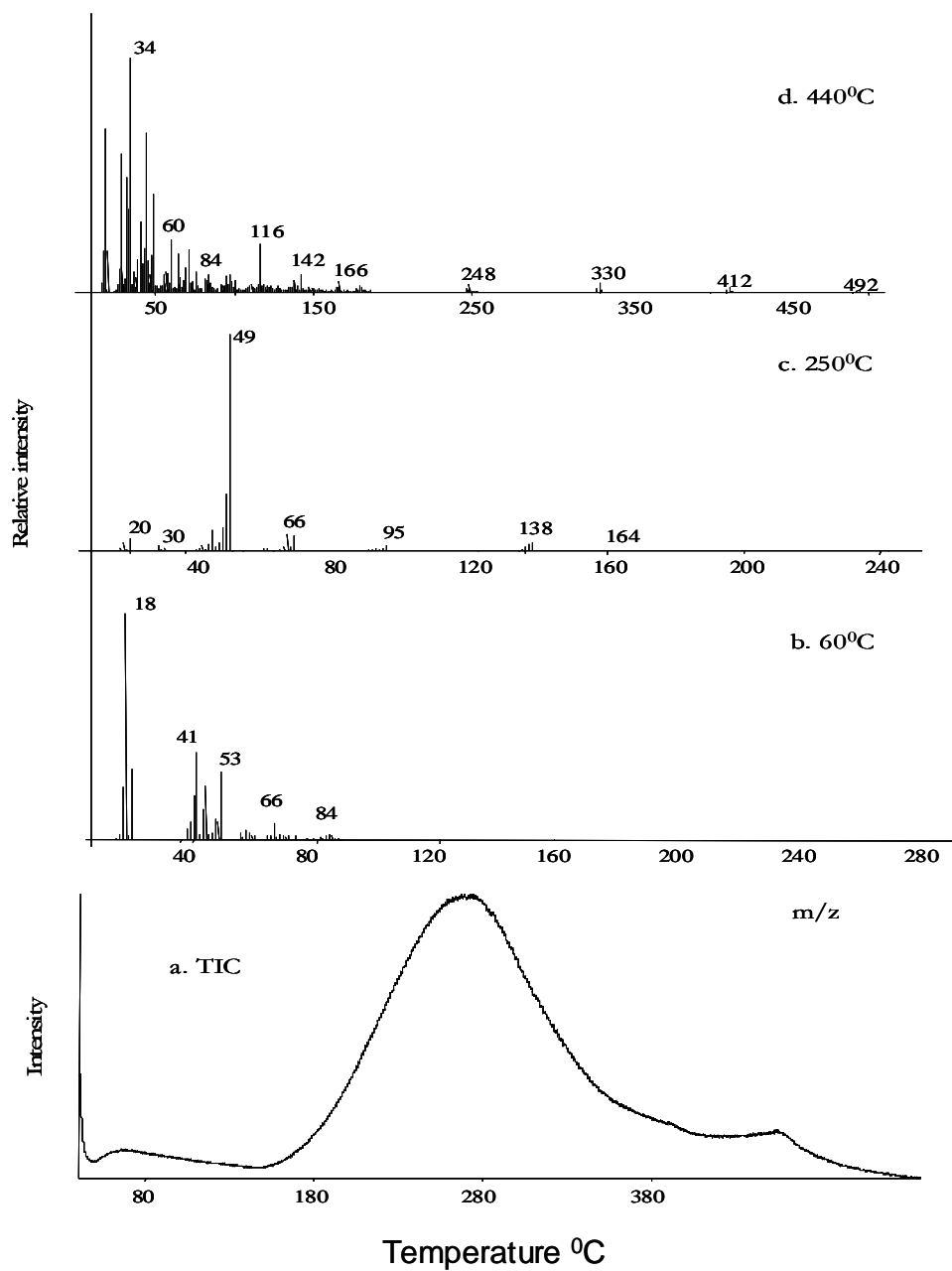


Figure 3.1 TIC curve and mass spectra recorded at temperatures corresponding to the maximum ion yield for PTh

Table 2 The characteristics and/or intense peaks present in the pyrolysis mass spectra corresponding to the maximum in the ion profiles recorded during the pyrolysis of PTh.

m/z	Assignments				
	19eV		70eV		
	250 °C	445 °C	250 °C	445 °C	
20	62	56	58	188	HF
28	34	370	23	614	CO, N ₂ , C ₂ H
30	4	31	11	28	BF, CH ₂ =O
32	10	380	3	475	S
34	4	1000	1	1000	H ₂ S
39	11	102	6	125	C ₃ H ₃
41	71	270	23	322	CH ₃ CN, C ₃ H ₅ , NC ₂ H ₃
44	193	435	91	644	CO ₂ , CS
45	44	111	20	135	CHS
49	1000	101	1000	404	BF ₂
60	54	324	15	240	OCS
64	21	98	8	148	SO ₂
68	95	70	74	50	BF ₃
83	6	54	1	37	C ₄ H ₃ S
84	21	117	3	74	Monomer
85	7	83	1	37	CH ₂ C ₄ H ₉ N
97	7	113	1	76	CH ₂ C ₄ H ₃ S
101	3	23		17	FC ₄ H ₂ S
102	2	18		9	FC ₄ H ₃ S
116	2	202	1	221	(C ₂ H ₂ S ₂) ₂
118	4	26	4	30	FC ₄ H ₂ (OH)S
122	2	21		19	C ₃ H ₃ C ₄ H ₃ S
138	67	37	39	57	C ₃ H ₃ C ₄ H ₂ (OH)S
142	6	112	1	73	(C ₄ H ₉) ₂ N=CH ₂ , (C ₃ H ₃ S) ₂
166		37		42	Dimer
179	2	22		18	C ₄ H ₃ SC ₄ H ₂ SCH ₂
185	3	23		10	(C ₄ H ₉) ₃ N
198		16		14	C ₄ H ₂ S(OH)C ₄ H ₂ S(OH)
204				8	C ₄ H ₃ SC ₄ H ₂ SC ₃ H ₃
207	2	13		9	C ₄ H ₃ SC ₄ H ₂ SCH ₂ CH ₂ CH ₂
242				4	(C ₄ H ₉) ₄ N
248		19		30	Trimer
330		39		41	Tetramer
412		19		26	Pentamer
494				3	Hexamer

In Figure 3.2 and 3.3, evolution profiles of some selected products are given. The single ion pyrograms of some dopant based products, such as HF ($m/z=20$ Da), BF_2 ($m/z=49$ Da), BF_3 ($m/z=68$ Da), counter ion Bu_4N^+ ($m/z=242$) and $(\text{C}_4\text{H}_9)_2\text{H}=\text{CH}_2$ ($m/z=142$ Da) are shown in Figure 3.2. BF_3 and BF_2 fragments showed identical trends and the maximum in the evolution profiles is at 250°C . Yet, HF generation was more efficient at low temperatures. It is known that reaction of BF_3 with H_2O yields HF. Thus, it may be proposed that HF is mainly produced due to reactions with adsorbed water. It is clear that the peak around 250°C in the TIC curve was due to the evolution of dopant and the peak above 400°C was due to the decomposition of PTh chains. Previous TGA and FTIR studies have shown that the degradation of PTh occurs in two steps (Figure 3.23.b). The first one is the weight loss in the temperature range $150\text{--}225^\circ\text{C}$ due to the removal of dopant ion and the second one is due to the degradation of the polymer itself [58,59]. Another point that was noted is the presence of peaks due to counter ion NBu_4^+ .

It can be observed from Figure 3.3 that the single ion pyrograms of low molecular weight of oligomers, dimer ($m/z=166$ Da), trimer ($m/z=248$ Da), tetramer ($m/z=330$ Da), pentamer ($m/z=412$ Da) and hexamer ($m/z=494$ Da) gave maximum around 445°C .

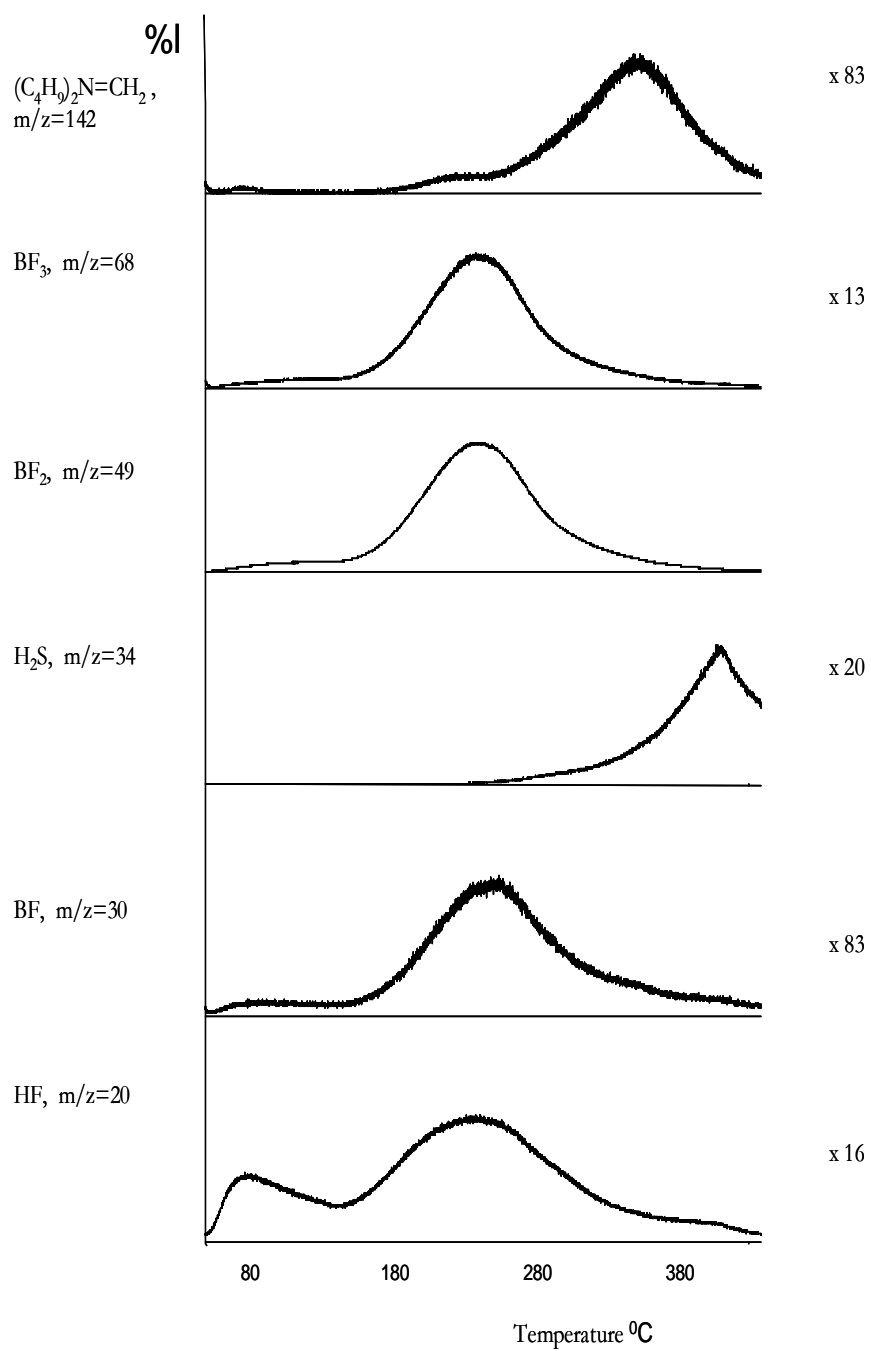


Figure 3.2 Single ion pyrograms of some selected fragments recorded during pyrolysis of PTh

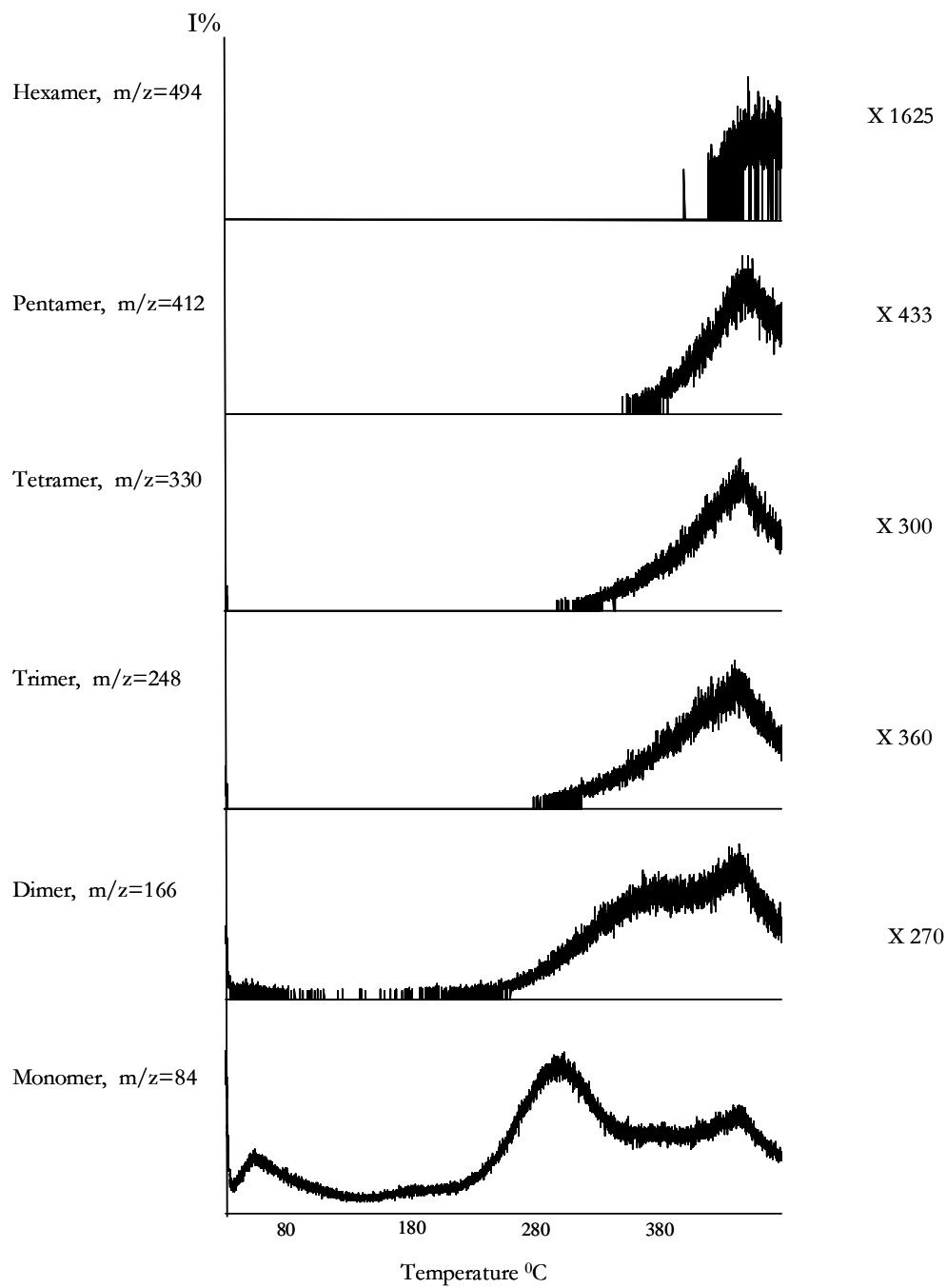


Figure 3.3 Single ion pyrograms of monomer and the oligomers at m/z 84, 166, 248, 330, 412, 494 obtained during the pyrolysis of PTh

3.2 DATE and Its Polymers

3.2.1 DATE

Pyrolysis mass spectra of DATE indicated evolution of the fragments readily below 500°C. In Figure 3.4 the mass spectrum of the monomer is shown. The molecular ion peak of DATE at $m/z=422$ Da was weak as expected for a large molecule involving labile bonds. The base peak was at $m/z=110$ Da and can directly be attributed to $C_4H_4SC_2H_3$ generated by the cleavage of the labile carbon oxygen bonds next to the C=O groups. Another high mass fragment peak was at 295 Da and was assigned to $C_4H_4SC_2H_4OCO(CH_2)_8CO$, again due to the cleavage of C-O bonds. Peaks that can readily be assigned to products due to the ruptures of the bonds next to C=O and β to the thiophene ring, and those stabilized by H-abstraction reactions were also present in the spectra. Furthermore, peaks due to decomposition of these fragments by elimination of small molecules such as CO, CO₂ and H₂O and peaks due to characteristic fragmentation pattern of thiophene ring were also significant in the spectra.

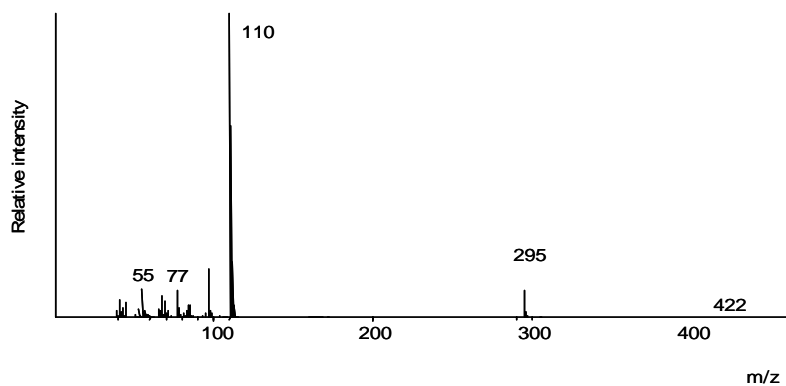
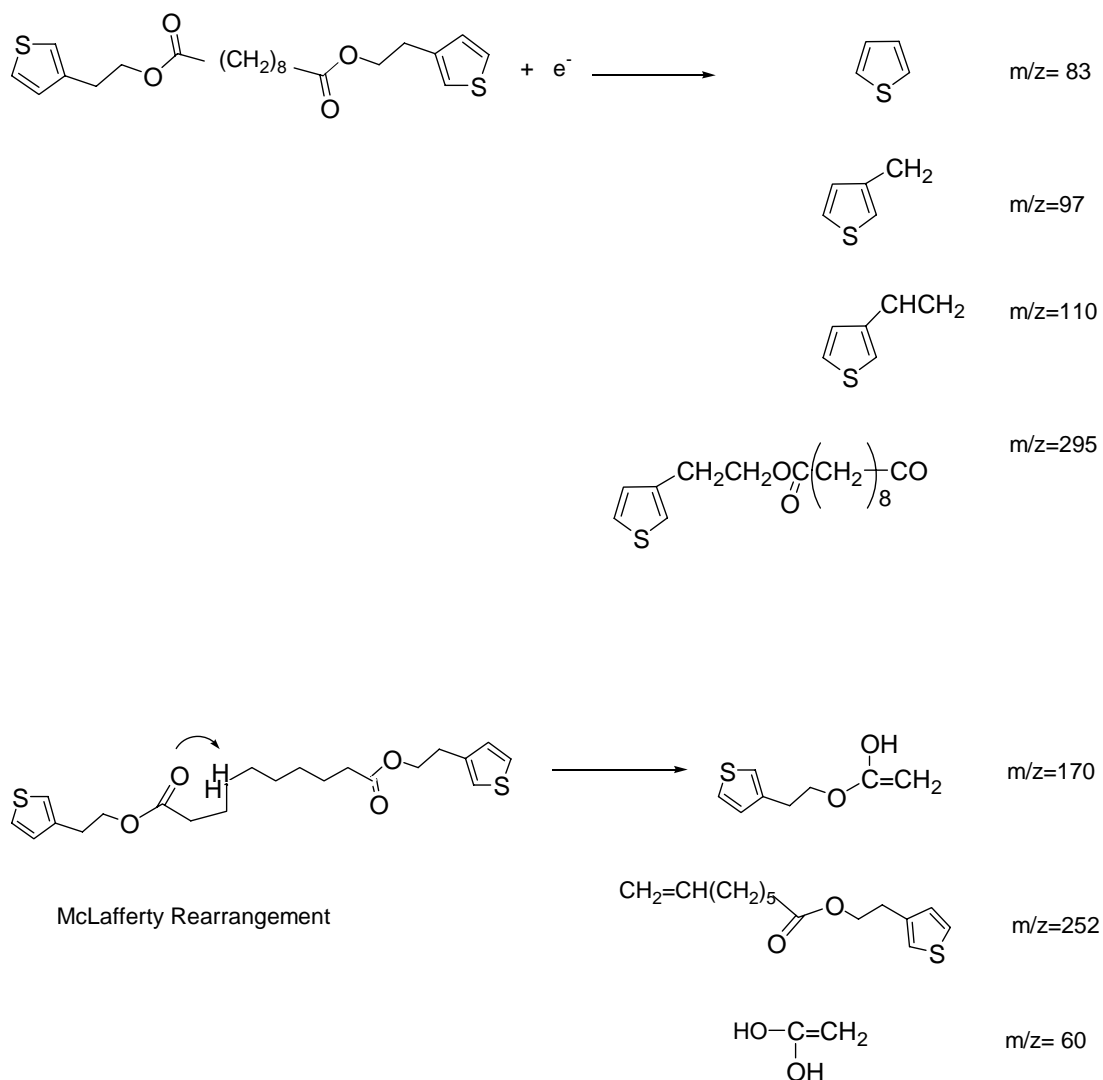


Figure 3.4 Mass spectra of DATE

Thus, the fragmentation observed in the mass spectrum is in accordance with the expected fragmentation pattern for DATE according to the general fragmentation rules (Scheme 4). The mass spectral data for DATE are summarized in Table 3.



Scheme 4. Proposed degradation products of DATE

3.2.2 Homopolymer of DATE (P(DATE))

The TGA curve of P(DATE) revealed two transitions at 232 and 433°C. Pyrolysis of P(DATE) yielded a total ion current, (TIC) curve (the variation of the total ion yield as a function of temperature) that also indicated a degradation mechanism involving mainly two steps (Figure 3.5). Yet, it can be noted from Figure 3.5 that, actually, the evolution of pyrolysis products started at initial stages of pyrolysis and continued throughout the process. Besides the two intense peaks at 275 and 440°C, weak peaks with maxima at 40, 75°C, and shoulders at 200 and 430°C were present in the TIC curve. The mass spectrum recorded at the maxima of the TIC curve are also included in the figure. In Table 4, the mass spectral data related to the intense and/or characteristic peaks in the pyrolysis mass spectra recorded at the maxima and the shoulders of the TIC curve are given. Presence of more than one peak in the TIC curve points out either the presence of more than one component in the sample or a multi step degradation mechanism. Actually, due to the doping process, all conducting polymers are multicomponent systems as they involve both the dopant ion and the matrix polymer.

The pyrolysis mass spectra recorded below 140°C involve peaks due to monomer and solvent adsorbed on the polymer. The dopant based fragment peaks due to BF₂, BF, HF were mainly detected below 270°C. Characteristic degradation products of polythiophene such as H₂S, HCS, thiophene and its dimer and trimer were recorded at elevated temperatures. Presence of thiophene dimer and although very weak, trimer confirmed polymerization reaction. Furthermore, peaks at m/z= 55, 69 and 98 Da that may readily be attributed to, C₄H₇, OCCH₂CHCH₂ and C₄H₃SCH₃ were quite intense. The fragmentation pattern recorded was drastically different than that of the monomer as expected. In general, degradation of a polymer via depolymerization reaction yielding mainly monomer is not likely when the monomer involves labile bonds. Thus, the pyrolysis mass spectra similar to that of the monomer were not observed for such polymers. Degradation of P(DATE) was observed in a broad temperature region, starting above 230°C and reaching to the maximum product yield around 440°C.

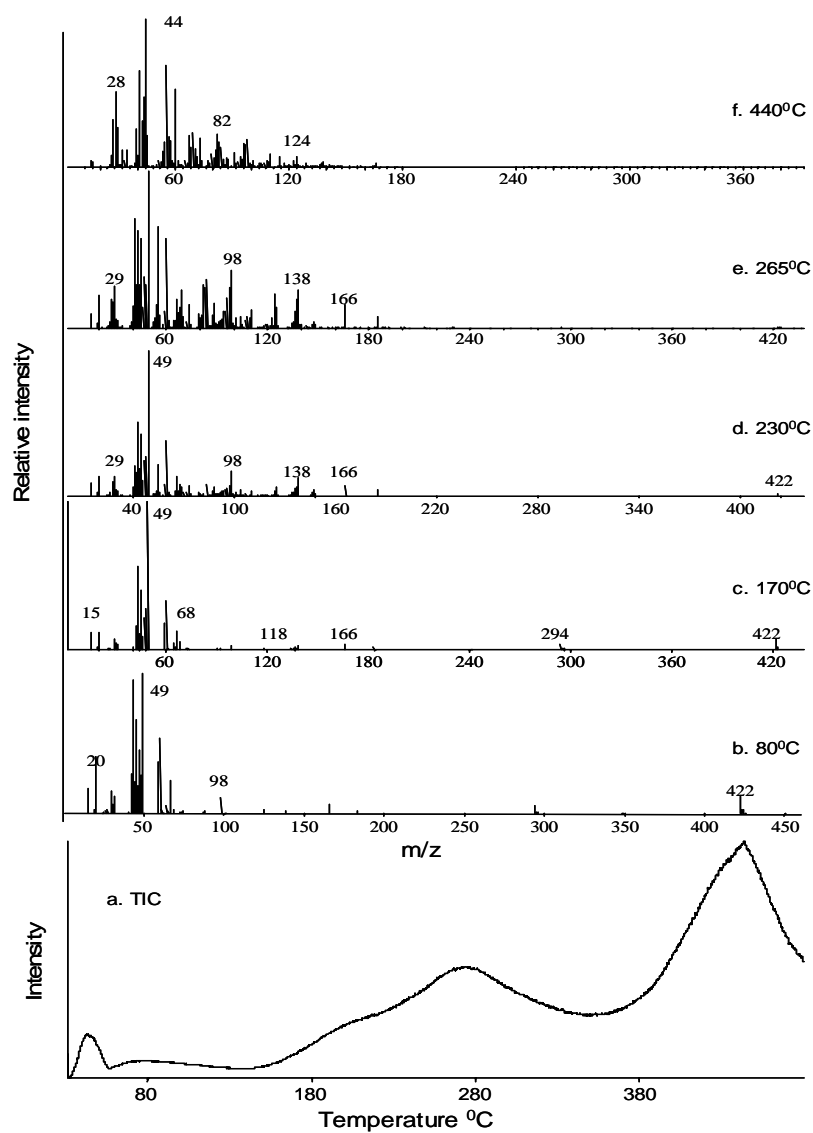


Figure 3.5 a .The TIC curve and the mass spectra recorded at b. 80°C, c. 170°C, d. 230°C, e. 265°C and f. 440°C

Table 3 The most and/or characteristic peaks of DATE and P(DATE) at some selected temperatures, with related chemical formula

m/z	P(DATE)			DATE		Assignments	
	70 eV		19 eV				
	200°C	270°C	440°C	270°C	440°C	125 °C	
18	362	516	628	313	455	11	H ₂ O
20	122	227	17	69	3		HF
30	49	65	23	28	18	1	BF, CH ₂ =O
34	6	19	111	23	147		H ₂ S
39	89	299	316	31	43	23	C ₃ H ₃
44	365	520	1000	469	1000	5	CO ₂ , CS
49	1000	1000	5	303			BF ₂
55	143	816	644	718	774	95	C ₄ H ₇
57	25	94	198	116	364	21	CHCS, C ₄ H ₉
66	133	190	30	130	21		BF ₂ OH
68	76	155	124	159	183		BF ₃
69	47	331	228	416	306	52	OCCH ₂ CHCH ₂
83	92	532	223	732	318	22	C ₄ H ₃ S
98	97	409	174	1000	477	21	C ₄ H ₃ SCH ₃
110	19	131	79	294	104	1000	C ₄ H ₃ SCHCH ₂
111	595	233	55	158	81	614	C ₄ H ₃ SCH ₂ CH ₂
124	23	281	69	432	122	1	C ₄ H ₃ SCHCO
125	35	137	25	303	64	4	C ₄ H ₃ SCH ₂ CO
128	24	36	22	35	16	8	C ₄ H ₃ SCH ₂ CH ₂ OH
138	82	261	34	355	79	2	C ₄ H ₃ SCH ₂ CHCO
154	4	10	7	16	8	1	OCOCH(CH ₂) ₅ CHCH ₂
166	50	166	29	235	53		Thiophene dimer
185	29	90	11	121	30		(C ₄ H ₉) ₃ N
212	1	4	2	4	2		OC(CH ₂) ₈ COOCH ₂ CH ₂
239	2	1	1		2	1	C ₄ H ₃ SCH ₂ CH ₂ OCO(CH ₂) ₆
240		3	2		2		H(CH ₂) ₆ OCOCH ₂ CH ₂ C ₄ H ₃ S
248			2	3	2		Thiophene trimer
267	16	4	1		1		C ₄ H ₃ SCOO(CH ₂) ₈ CO
282			1		1	3	OC ₂ H ₄ C ₄ H ₂ SC ₄ H ₂ SC ₂ H ₄ OCO
295					1	138	C ₄ H ₃ SCH ₂ CH ₂ COO(CH ₂) ₈ CO
422	32	6				3	Monomer

To get a better insight, in Figure 3.6 single ion pyrograms of products diagnostic to dopant (BF_2 at $m/z=49$ Da), monomer (monomer at $m/z=422$ Da) and thiophene bearing fragments ($\text{C}_4\text{H}_3\text{SCH}_3$ at $m/z=97$ Da, thiophene dimer at $m/z=166$ Da, thiophene trimer at $m/z=248$ Da) are shown. Evolution profiles of H_2S at $m/z=34$ Da, CO_2 at $m/z=44$ Da and fragments involving units of the ester chain such as C_4H_7 at $m/z=55$ Da, $\text{OCCH}_2\text{CHCH}_2$ at $m/z=69$ Da are also included in the figure.

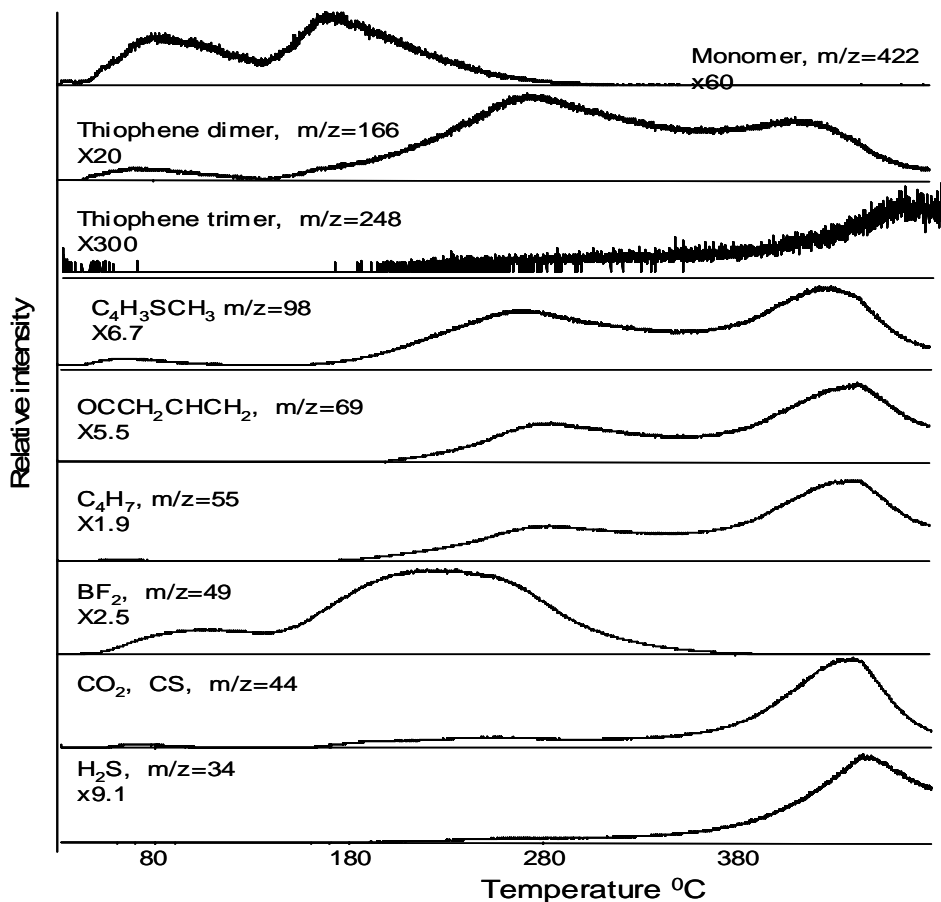
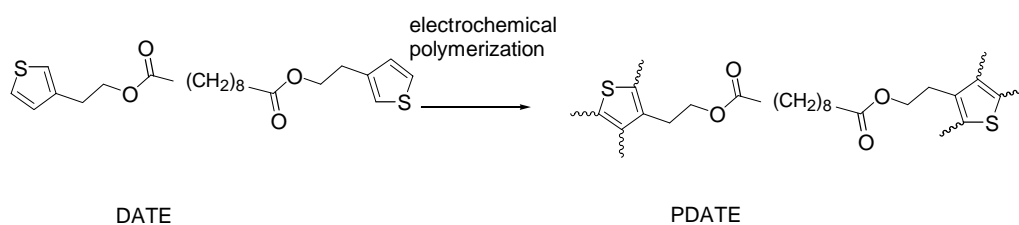


Figure 3.6 Single ion pyrograms of some selected fragments recorded during pyrolysis of P(DATE)

Inspection of single ion pyrograms revealed that dopant evolution has occurred in two regions as in the case of polythiophene. It has been proposed that physically adsorbed dopant readily evolves below 100⁰C, whereas dopant leaves the polymer around 230⁰C. The degradation of the polymer also occurred in two temperature regions. It is clear that decomposition started by the cleavage of labile bonds along the ester linkages connecting the thiophene units. Though dimer yield was high around 270⁰C, trimer and low molecular weight species indicating cleavage of the thiophene ring were mainly generated at elevated temperatures. H₂S formation from thiophene itself is not detected; yet, it is produced during the pyrolysis of polythiophene at elevated temperatures. The high temperature evolution of H₂S was related to the network structure of thiophene for which decomposition of the thiophene ring should be more likely. Thus, it may be proposed that due to the substitution at 3- position, chain growths from both 2 and 5 positions were inhibited to a certain extent (Scheme 5). However, as the monomer involves two thiophene units at both ends, a thermally unstable polymer has been produced which decomposes at around 275⁰C. The chains produced by the growth of polythiophene at both 2 and 5 positions degraded around 440⁰C. The network structure of these chains was confirmed by the presence of intense H₂S and CS peaks. The proposed polymerization process is in accordance with pyrolysis mass data.



Scheme 5 Proposed electrochemical polymerization route

3.2.3 Copolymers of DATE with Thiophene

In this section, the results of direct insertion probe pyrolysis mass spectrometry analyses of electrochemically prepared P(DATE-co-Th) films and the mechanical mixture of PTh and P(DATE) were discussed.

The total ion current (TIC) curves recorded during the pyrolysis of electrochemically prepared P(DATE-co-Th) the mechanical mixture and the corresponding homopolymers P(DATE) and PTh are shown in Figure 3.7. Though, some changes in the relative intensities of the peaks present in the TIC curves are recorded, for all the samples the TIC curves show three peaks in similar temperature ranges indicating either a multistage degradation mechanism or presence of more than one component. The most significant point is the low intensity of the second peak in the TIC curve of P(DATE-co-Th). To get a better insight, pyrolysis mass spectra recorded at the maxima of the peaks in TIC curve were studied. The pyrolysis mass spectra of both P(DATE-co-Th) and the mechanical mixture were dominated with diagnostic peaks of both PTh and P(DATE). The pyrolysis mass spectra recorded at the maxima of the TIC curves of P(DATE-co-Th) is shown in Figures 3.8. It is clear that pyrolysis mass spectra were dominated with similar peaks that are diagnostic to PTh and P(DATE).

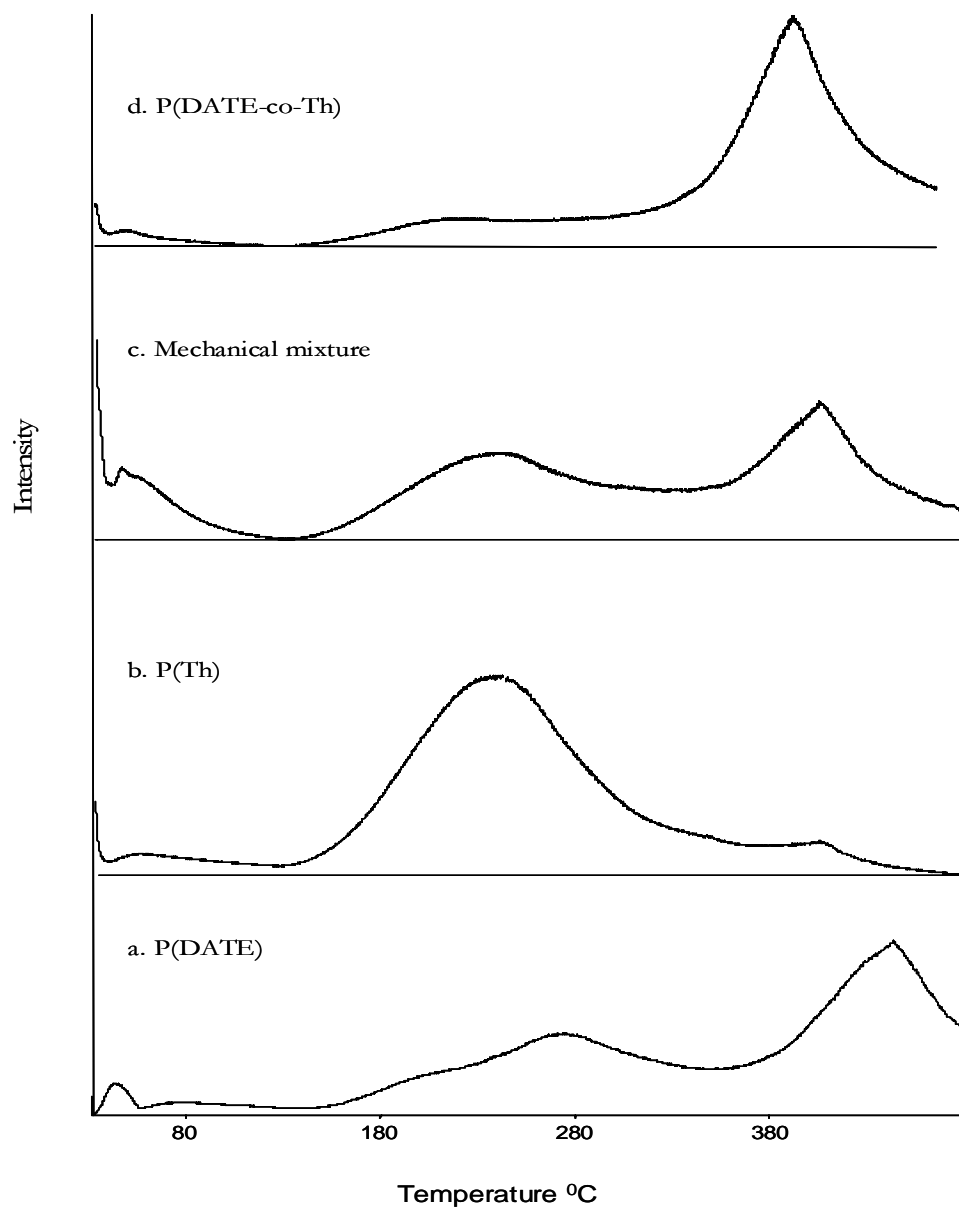


Figure 3.7 TIC curve recorded during the pyrolysis of a. P(DATE), b. PTh, c. mechanical mixture corresponding homopolymers d. P(DATE-co-Th)

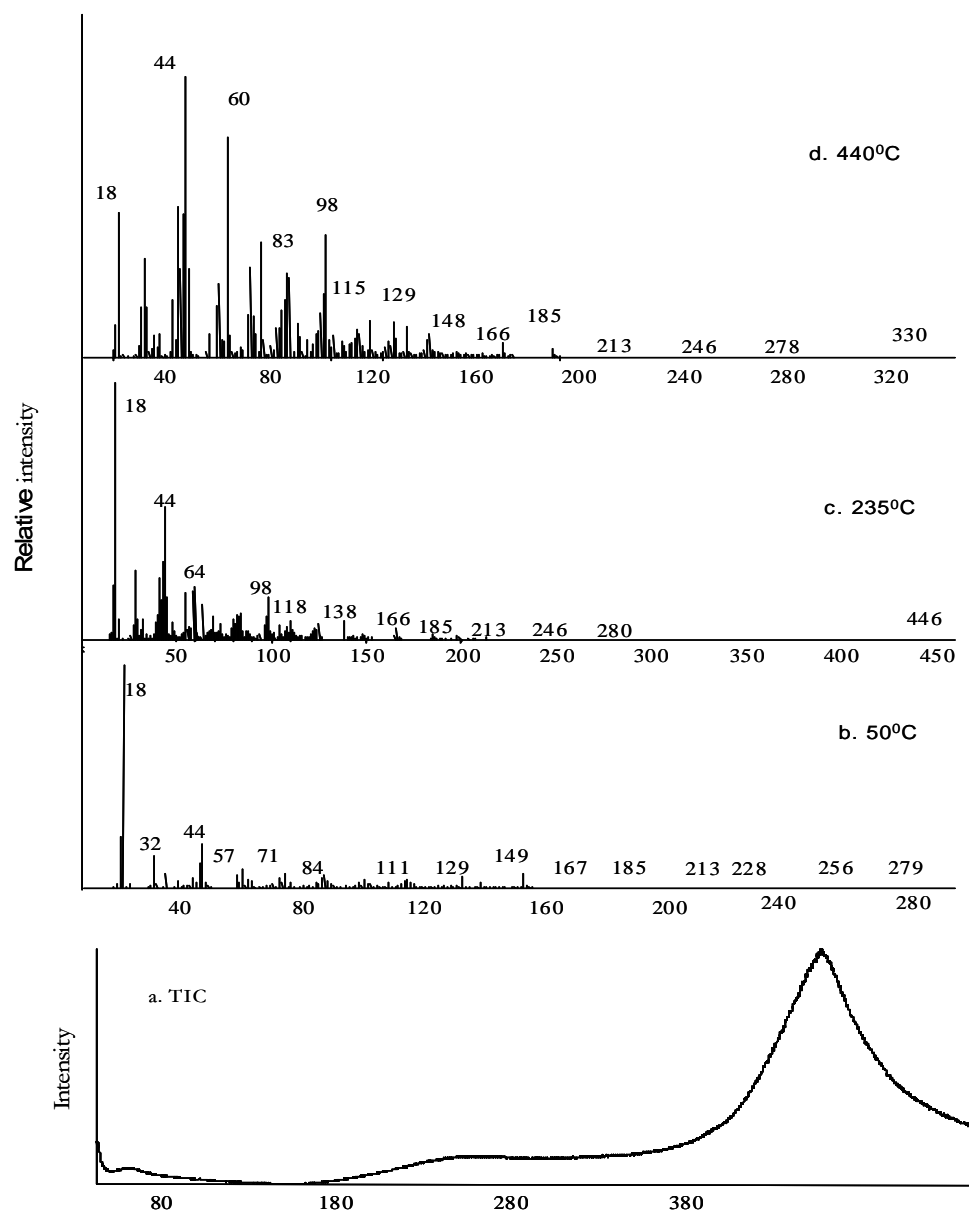


Figure 3.8 a .The TIC curve and the mass spectra recorded at b. 50°C, c. 235°C, d. 440°C

The evolution profiles of all characteristic thermal decomposition products generated during the pyrolysis of P(DATE-co-Th) and compared with those recorded from the corresponding homopolymers. The single ion pyrograms of these products recorded during the pyrolysis of P(DATE-co-Th) are given in Figure 3.9.

One of the most significant differences noticed was the decrease in the relative intensities of dopant based peaks that are recorded at initial stages and around 225 °C. Actually, the mole ratio of dopant/total monomer was lower during the synthesis of the copolymer. Thus, it is reasonable to obtain a lower extent of doping for the copolymer. The yields of thiophene trimer, $\text{H}_2\text{S OCCH}_2\text{CHCH}_2$ and thiophene were compared to get a better understanding. It can be concluded that trimer / thiophene ratio increases in the order PTh > Co > PDATE. Furthermore, trimer yield was higher for the copolymer with respect to $\text{OCCH}_2\text{CHCH}_2$ fragment yield. These results indicated that polythiophene chains were present in the copolymer sample. Another point recorded was the decrease in the relative intensities of DATE based fragments around 275 °C. This may point out that low molecular weight DATE oligomers or DATE terminal groups were decreased in the copolymer. This may further indicate growth of thiophene on DATE confirming copolymer formation.

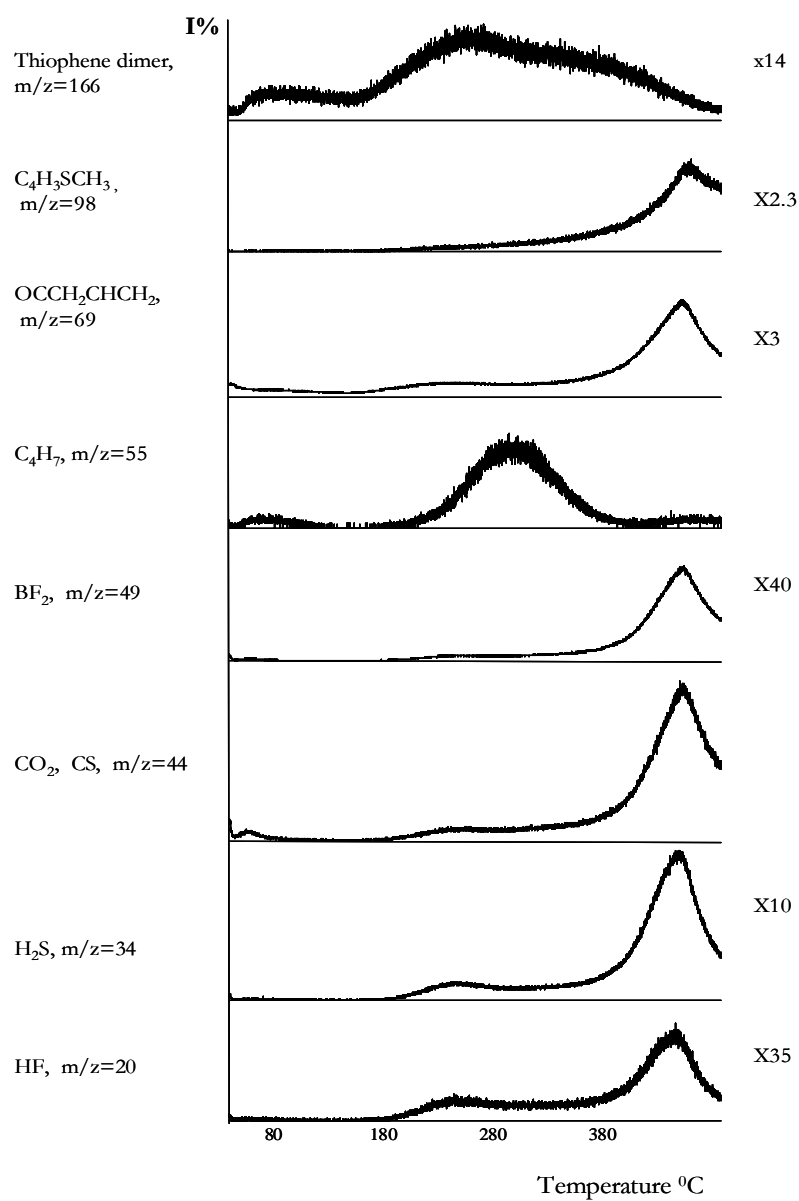


Figure 3.8 The ion-temperature profiles of most intense and characteristic peaks as a function of temperature observed during pyrolysis of P(DATE-co-Th)

Table 4 The most and/or characteristic peaks of P(DATE-co-Th) at some selected temperatures, with related chemical formula

m/z	P(DATE-co-Th)				Assignments		
	70 eV			19 eV			
	50°C	250°C	445°C	50°C	250°C	445°C	
20	16	81	6		13	3	HF
30	5	15	19	8	5	13	BF, CH ₂ =O
34	2	16	91	7	11	145	H ₂ S
39	16	65	219	8	9	48	C ₃ H ₃
44	185	476	1000	172	132	663	CO ₂ , CS
49	6	29	2	11	16		BF ₂
55	60	171	913	43	48	804	C ₄ H ₇
57	76	45	267	84	14	376	CHCS, C ₄ H ₉
66	11	19	27	28	7	22	BF ₂ OH
68	11	29	161	15	11	201	BF ₃
69	38	92	326	40	27	361	OCCH ₂ CHCH ₂
83	42	88	297	52	30	366	C ₄ H ₃ S
98	15	164	443	29	68	646	C ₄ H ₃ SCH ₃
110	29	67	95	46	28	112	C ₄ H ₃ SCHCH ₂
111	38	39	81	52	14	94	C ₄ H ₃ SCH ₂ CH ₂
124	6	36	130	11	11	122	C ₄ H ₃ SCHCO
125	16	58	69	31	20	126	C ₄ H ₃ SCH ₂ CO
128	8	14	18	10		18	C ₄ H ₃ SCH ₂ CH ₂ OH
138	7	74	81	11	18	130	C ₄ H ₃ SCH ₂ CHCO
154	5	5	11	8		11	OCOCH(CH ₂) ₅ CHCH ₂
166	6	40	56	7	4	88	Thiophene dimer
167	24	14	12	41		16	HOCCH(CH ₂) ₇ COOC(CH ₈)CO
185	8	28	36		10	42	(C ₄ H ₉) ₃ N
239	4		2			2	C ₄ H ₃ SCH ₂ CH ₂ OCO(CH ₂) ₆
248		20	4		4	4	Thiophene trimer

3.2.4 Thermal Gravimetric Analysis of DATE

As shown in Figure 3.9.a, TGA curve of DATE showed single weight loss at 376°C. The TGA curve for homopolymer revealed two transitions at 232°C and 433°C. The former weight loss could be attributed to the removal of the dopant ion, the latter could be due to decomposition of the polymer matrix (Figure 3.9.b). The char residue of PTATE was 39 % after 830°C. However, 2 % of TATE remained after 630°C. In the case of copolymer, thermogravimetry showed several patterns weight loss at 80°C due to entrapped solvent and monomer, at 230°C due to the removal of dopant ion and at 430°C due to decomposition (Figure 3.9.c) [56].

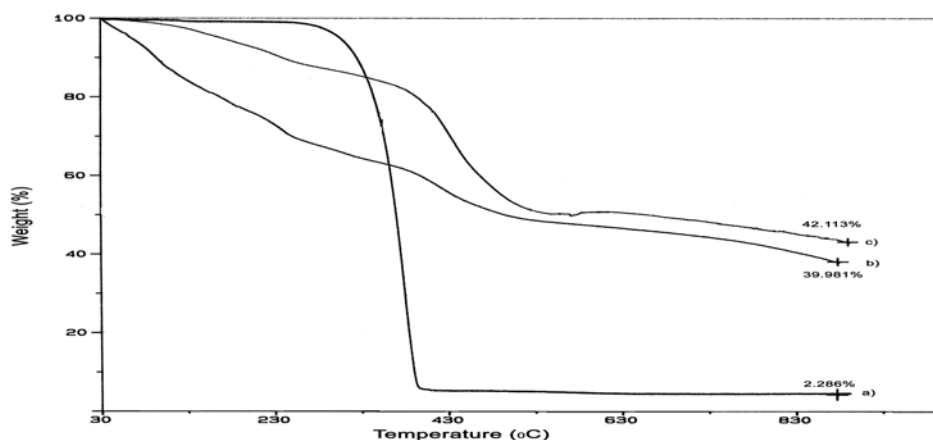


Figure 3.9 TGA thermogram (a) DATE (b) P(DATE) (c)P(DATE-co-Th)

3.2.5 Conductivity Measurements

The conductivity of P(DATE) was measured as 1.2×10^{-3} S/cm according to four probe technique. For the copolymer with thiophene this value was determined to be 8×10^{-2} S/cm.

3.1 TATE and Its Polymers

3.1.1. TATE

Pyrolysis mass spectra of the monomer, TATE indicated evolution of the monomer readily below 50⁰C. In Figure 3.10 the mass spectrum of the monomer is shown. The molecular ion peak of TATE at $m/z=386$ Da was weak and the base peak was at $m/z=110$ Da due to $C_4H_4SC_2H_3$. Other intense peaks due to the cleavage of labile C-O bonds were at $m/z=149$, and 259 Da is assigned to $C_2H_4OCOC_6H_5$ and $C_4H_3SCH_2CH_2OCOC_6H_4CO$ respectively. Diagnostic peaks of thiophene ring, CO, CO₂ and H₂O were also present. The degradation products are shown in Scheme 6 and the mass spectral data for TATE are summarized in Table 5.

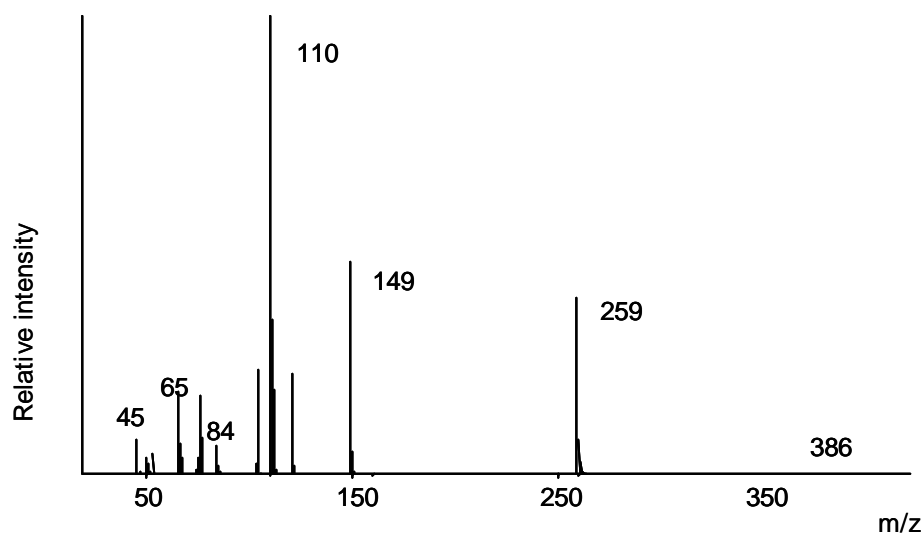
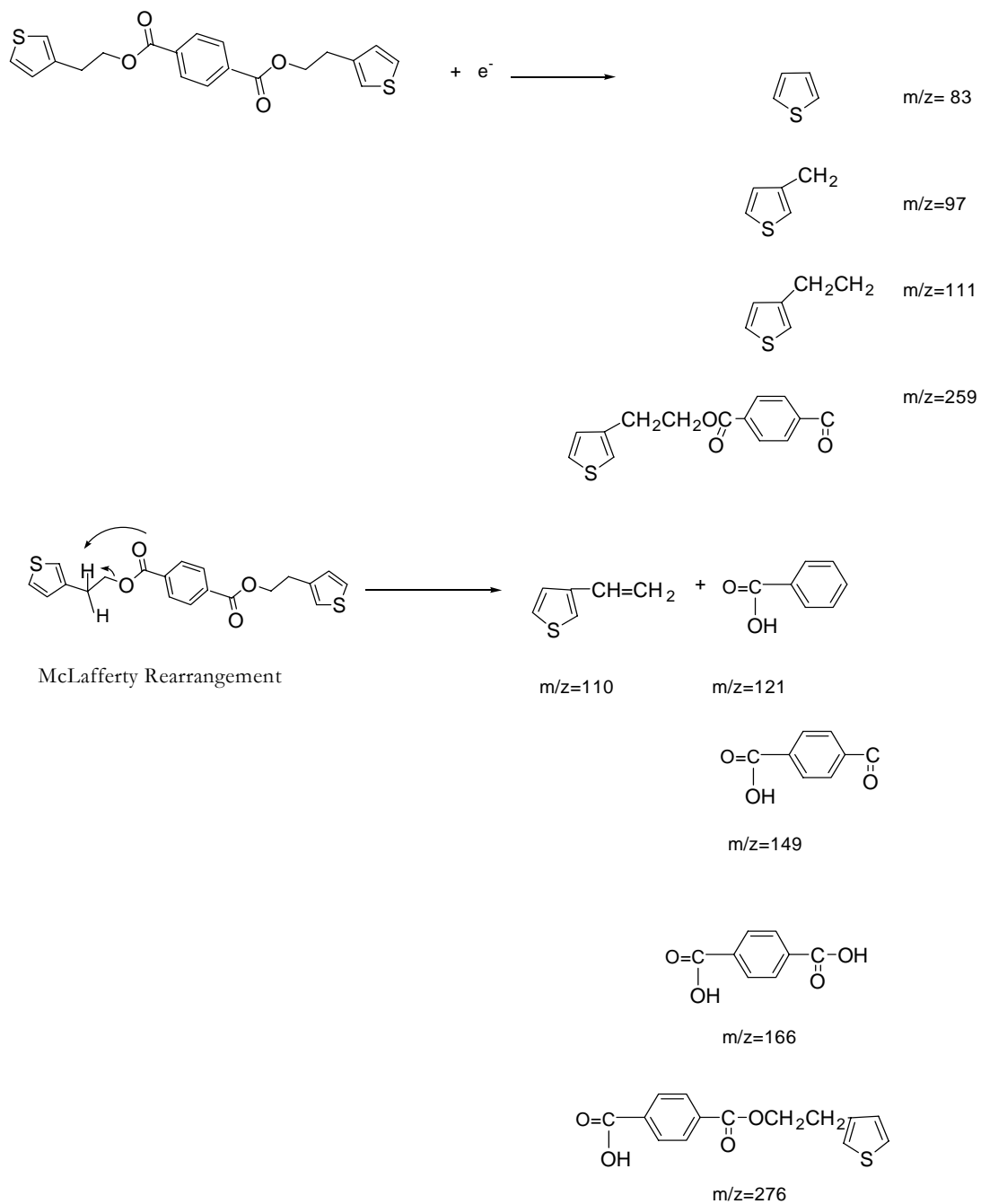


Figure 3.10 Mass spectra of TATE



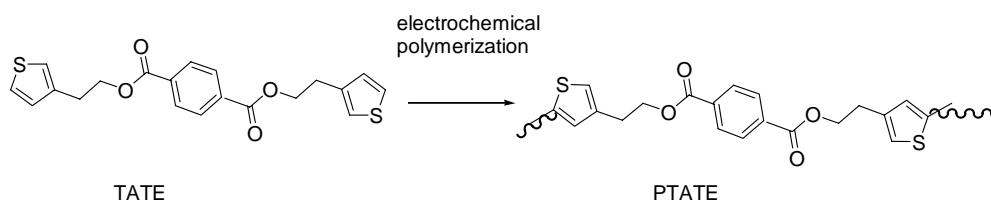
Scheme 6 The degradation products of TATE

3.1.2 Homopolymer of TATE (P(TATE))

The total ion current (TIC) curve that is the variation of total ion intensity as a function of temperature of P(TATE) is given in Figure 3.11. Pyrolysis of P(TATE) showed two weak peaks at 78 and 210⁰C and an intense peak at 430⁰C and these three peaks can be seen in the TIC curve and the related mass spectral data are collected in Table 6. No monomer peak was detected for this polymer. The mass spectra recorded below 250⁰C are mainly dominated with peaks diagnostic to dopant. Peaks that may be attributed to polymer degradation were only detected in the final stages of pyrolysis. In Figure 3.12 evolution profiles of characteristic and/or intense fragments are shown. Again, evolution of dopant occurred nearly in the same region with those of PTh, P(DATE) and P(OTE). However, significant changes were observed in the degradation behavior of P(TATE) compared to P(DATE). The degradation of polymer occurred in one step at elevated temperatures unlike P(DATE). Again, fragments indicating the cleavage of the ester linkage were intense. The high temperature shift can be associated with the increase in thermal stability of ester linkage when hydrocarbon chain was replaced by C₆H₄ group. On the other hand, presence of a single peak for polymer decomposition may be attributed to a uniform structure.

Another point of interest was the lack of thiophene trimer peak, though the dimer yield was significantly high. Furthermore, H₂S and CS peaks were diminished drastically indicating a pronounced decrease in the extent of network structure compared to P(DATE). It may be thought that in the case of P(TATE), the presence of more stable and rigid ester linkages involving phenyl group inhibits coupling of thiophenes at 2 position. If the coupling at 2 positions were inhibited, then thiophene trimer should not be present and a network structure should be formed. Thus, it may be concluded that the growth of P(TATE) mainly occurred through both thiophene ends by the coupling of thiophene moieties at 5 positions (Scheme 7).

Such a structure should bring a decrease in conductivity, as the delocalization of the dopant anions should also be restricted. The conductivities of P(DATE) and P(TATE) were measured as 1.2×10^{-3} and $4 \times 10^{-5} \text{ S.cm}^{-1}$ respectively. The dopant and polymer based peaks were recorded to have comparable ratios for both P(DATE) and P(TATE). Thus, the low conductivity value for P(TATE) also supports the proposed structure for P(TATE). The proposed polymerization process for P(TATE) in accordance with pyrolysis data.



Scheme 7 Proposed electrochemical polymerization route

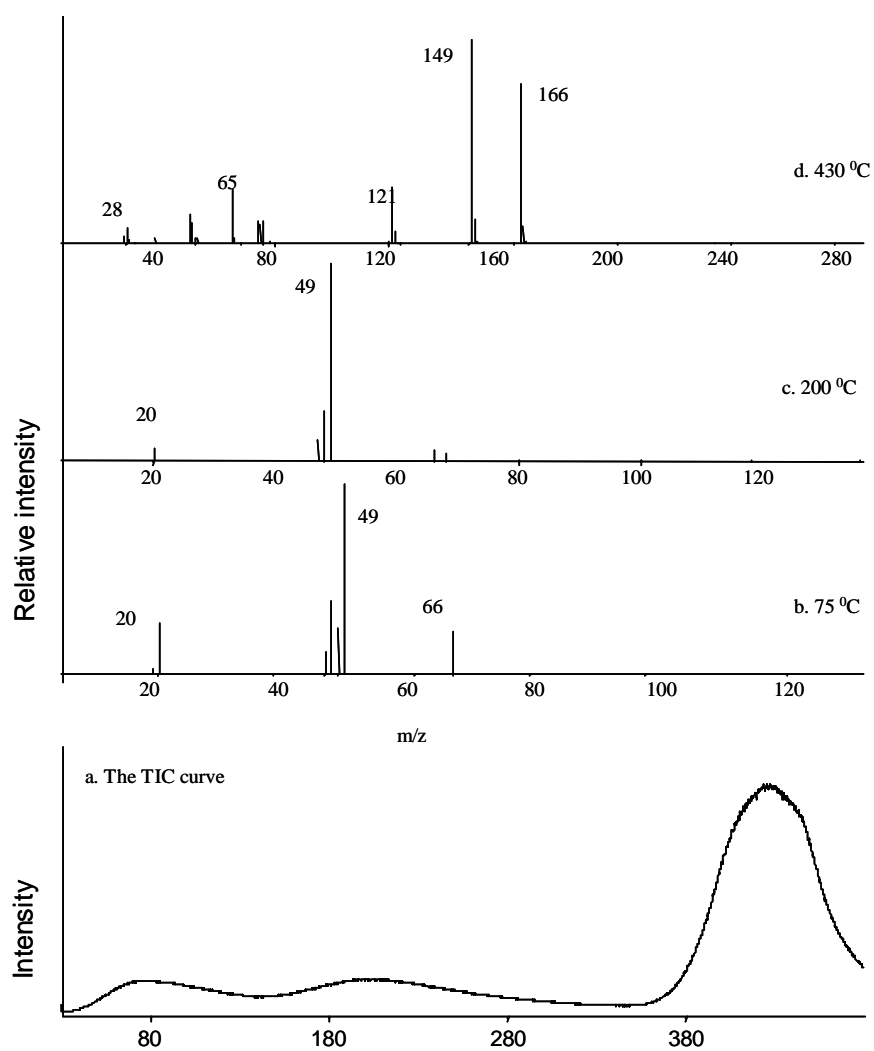


Figure 3.11 a.The TIC curve and the mass spectra recorded at b. 75°C, c. 200°C, and d. 430°C

Table 5 The most and/or characteristic peaks of TATE and P(TATE) at some selected temperatures, with related chemical formula

m/z	P(TATE)			TATE		Assignments	
	70 eV			19 eV			
	60°C	200°C	440°C	330°C	440°C		
18	588	256	329	242	49		H ₂ O
20	286	105	8	7			HF
30	22	16	3	23	1		BF, CH ₂ =O
34			25	44	21		H ₂ S
39	25	26	98	88	31	37	C ₃ H ₃
44	78	76	83	328	39		CO ₂ , CS
49	1000	1000	14	48			BF ₂
55	12	7	29	100	11	3	C ₄ H ₇
57	12	10	10	184	5	7	CHCS, C ₄ H ₉
65	58	17	266	200	231	181	C ₅ H ₅
66	224	62	27	17	17		BF ₂ OH
68	62	62	2	35	2		BF ₃
76		1	103	32	28	168	C ₆ H ₄
77	3	3	85	51	72	87	C ₆ H ₅
83	20	26	4	26	2	7	C ₄ H ₃ S
84	6	6	5	57	3	71	C ₄ H ₄ S
93	5	5	37	40	36	27	C ₆ H ₄ OH
97	7	5	4	69	3	264	C ₄ H ₃ SCH ₂
104		1		27	21	232	C ₆ H ₄ CO
105	3	2	65	21	70	27	C ₆ H ₄ COH
110	3	2	6	29	3	1000	C ₄ H ₃ SCHCH ₂
111	185	304	7	26	4	357	C ₄ H ₃ SCH ₂ CH ₂
121	6	4	286	246	263	221	C ₆ H ₄ COOH
125	2	2	1	16	2		C ₄ H ₃ SCH ₂ CO
128	18	10	3	17	1	5	C ₄ H ₃ SCH ₂ CH ₂ OH
149	8	5	1000	1000	1000	490	HOCOC ₆ H ₄ CO
166	2	8	760	880	931	5	C ₄ H ₃ SC ₄ H ₃ S
185		2	1	7	1		(C ₄ H ₉) ₃ N
259						384	C ₄ H ₃ SCH ₂ CH ₂ COOC ₆ H ₅ CO
386						0.5	Monomer

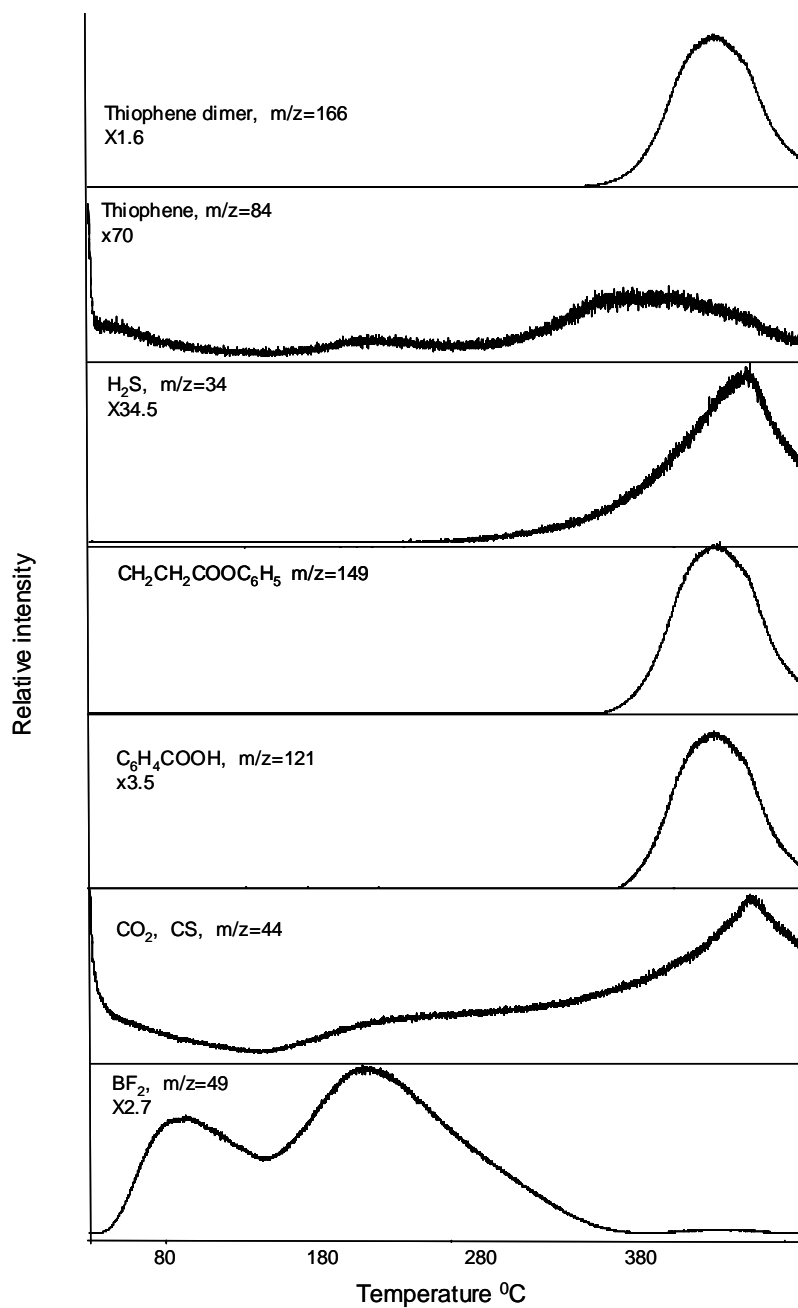


Figure 3.12 The ion-temperature profiles of most intense and characteristic peaks as a function of temperature observed during pyrolysis of P(TATE)

3.1.3 Copolymer of TATE with Thiophene

In this section, electrochemically prepared P(TATE-co-Th) films and mechanical mixture of PTh and P(TATE) were studied by utilizing direct insertion probe pyrolysis mass spectrometry technique.

The total ion current (TIC) curve recorded during the pyrolysis of electrochemically prepared P(TATE-co-Th) film is shown in Figure 3.13, together with the TIC curves for the mechanical mixture and the corresponding homopolymers P(TATE) and PTh. P(TATE-co-Th) shows almost an identical trend with that of P(TATE). Furthermore, the pyrolysis mass spectrum recorded at the temperature corresponding to maximum ion yield is also quite similar to that of P(TATE) (Figure 3.14). In order to determine the effect of dissociative ionization, the pyrolysis experiments were repeated while decreasing ionization energy from 70 to 19 eV. The data for P(TATE-co-Th) products during pyrolysis for both 19 and 70 eV are included in Table 6. For both mass spectra recorded at 70 and 19 eV TIC curves showed similar trends. Furthermore, both of the 70 and 19 eV, pyrolysis mass spectra were dominated with the same product peaks. The relative intensities of the peaks in the TIC curve and the product peaks in the pyrolysis mass spectra have changed significantly. Thus, it can be concluded that the dissociative ionization in the mass spectrometer was quite important. However, fragmentation pattern recorded at elevated temperatures are quite similar. It may be thought that dissociative ionization in the mass spectrometer has no importance on analyses on thermal degradation of the polymer.

Analyses of both 70 and 19 eV pyrolysis mass spectra indicated that at initial stages of pyrolysis, at temperature lower than 100°C, mainly, the evolution of the solvent, acetonitrile, water and adsorbed dopant and its counter ion Bu_4N^+ have occurred. Evolutions of dopant based products were observed in the temperature region of 120°C to 340°C. The most intense fragment is BF_2^+ ($m/z=49$ Da), and its maximum yield

was observed at 240⁰C. Peaks that can be associated with thermal degradation of P(TATE-co-Th) were detected in the final stage of pyrolysis.

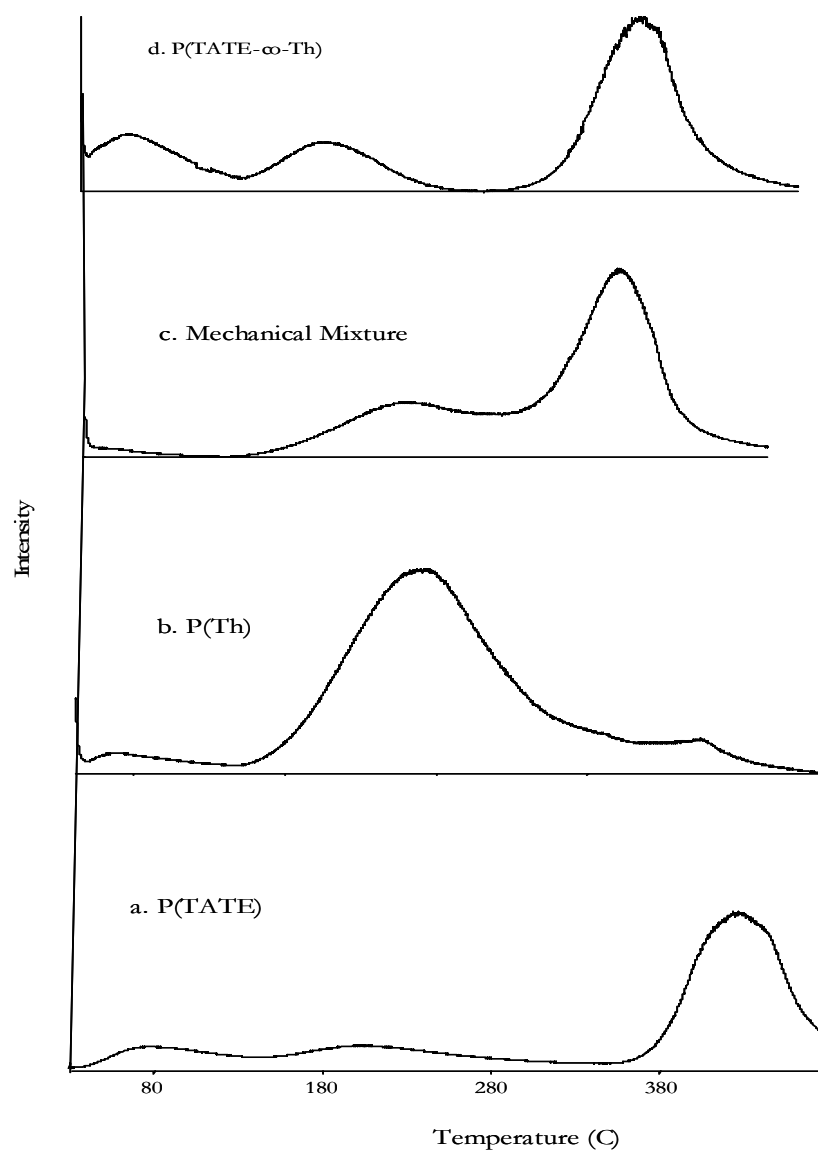


Figure 3.13 TIC curve recorded during the pyrolysis of a. P(TATE), b. P(Th), c. mechanical mixture and d. P(TATE-co-Th)

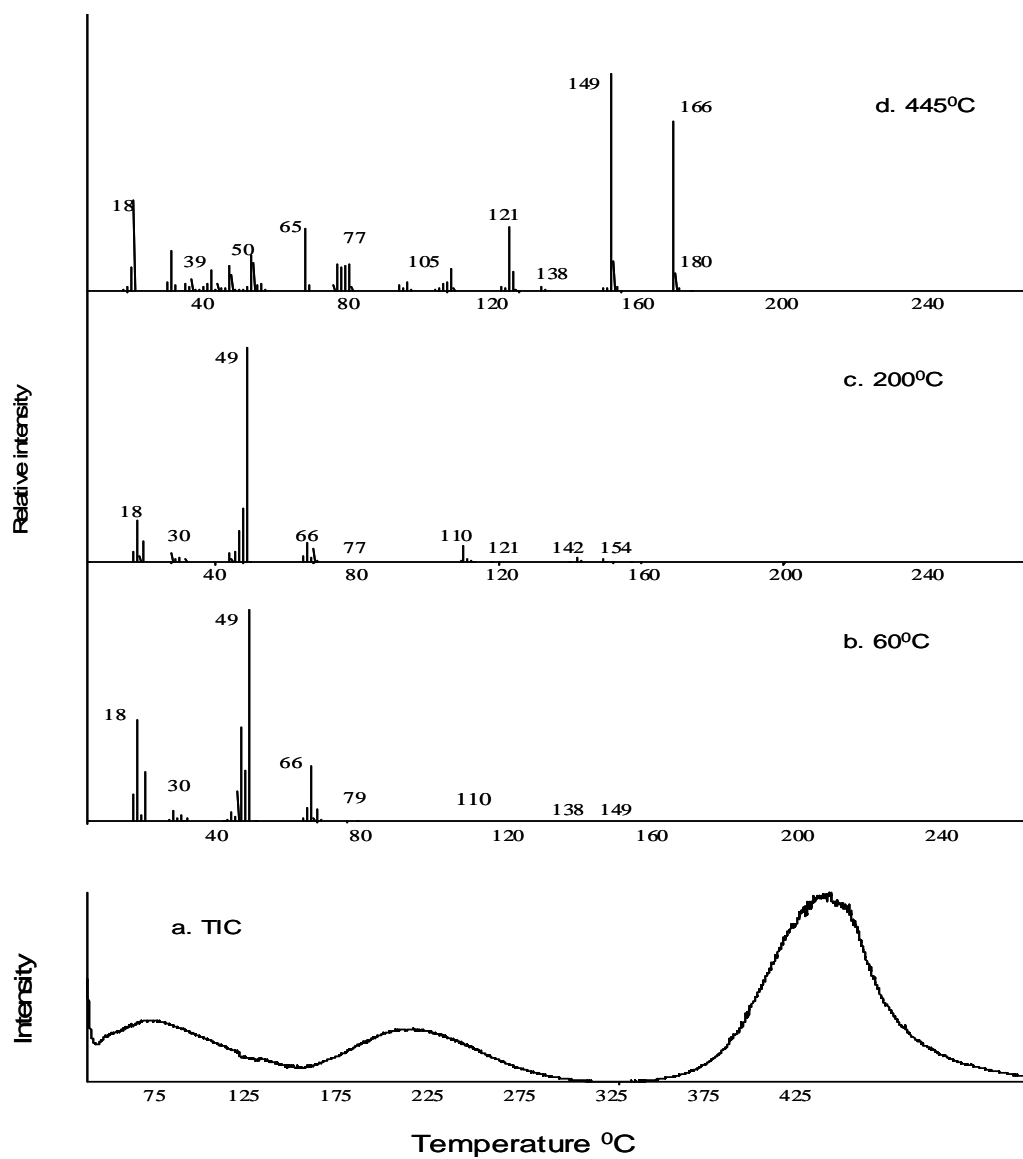


Figure 3.14 a. The TIC curve and the mass spectra recorded at b. 60°C, c. 200°C, and d. 445°C during the pyrolysis of P(TATE-co-Th)

Table 6. The most and/or characteristic peaks of P(TATE-co-Th) at some selected temperatures, with related chemical formula

m/z	P(TATE-co-Th)					Assignments	
	70 eV			19 eV			
	60°C	200°C	440°C	50°C	230°C	440°C	
18	503	187	414	1000	283	50	H ₂ O
20	233	95	11				HF
28	47	37	179	161	1000	124	N ₂
30	27	21	4			1	BF, CH ₂ =O
34	1	10	51	2	90	98	H ₂ S
39	4	4	90	14		26	C ₃ H ₃
44	44	41	115	176	310	40	CO ₂ , CS
49	1000	1000	16		14		BF ₂
55	7	4	18	80	35	6	C ₄ H ₇
57	7	5	9	72	58	4	CHCS, C ₄ H ₉
65	66	25	286			221	C ₅ H ₅
66	260	87	30			17	BF ₂ OH
68	59	60	2	23		2	BF ₃
76	1	4	114			25	C ₆ H ₄
77	3	3	124	16		56	C ₆ H ₅
83	4	2	2	31	20	1	C ₄ H ₃ S
84	2	3	7	66	44	3	C ₄ H ₄ S
93	4	2	39			31	C ₆ H ₄ OH
97	4	6	4	31	19	3	C ₄ H ₃ SCH ₂
104	1	5	44			24	C ₆ H ₄ CO
105	3	2	105	25		44	C ₆ H ₄ COH
110	10	74	6	47	42	5	C ₄ H ₃ SCHCH ₂
111	7	12	4	33	13	2	C ₄ H ₃ SCH ₂ CH ₂
121	3	5	291			266	C ₆ H ₄ COOH
125	1		1	12			C ₄ H ₃ SCH ₂ CO
128	1	1	2	18	17		C ₄ H ₃ SCH ₂ CH ₂ OH
149	6	11	1000	31	24	1000	HOCOC ₆ H ₄ CO
166	1		774			959	C ₄ H ₃ SC ₄ H ₃ S
185	1	3	4	23	80		(C ₄ H ₉) ₃ N
259	1	6					C ₄ H ₃ SCH ₂ CH ₂ COOC ₆ H ₅ CO

Actually, the analyses of pyrolysis data were quite complicated since degradation of P(TATE-co-Th) yielded several products over a wide temperature range. Thus, the trends in evolution profiles have to be analyzed in detail. In order to investigate the effect of each component on the characteristics of the other, the single ion pyrograms of characteristic thermal decomposition products of polythiophene and P(TATE) chains generated during the pyrolysis of P(TATE-co-Th) were studied and compared with those recorded for the corresponding homopolymers.

In Figure 3.15, the time-temperature resolved ion curves of products that are attributed to mainly the matrix (thiophene dimer $m/z=166$ Da, thiophene $m/z= 84$ Da, H_2S $m/z=34$ Da, $CH_2CH_2COOC_6H_5$ $m/z=149$ Da, C_6H_4COOH $m/z= 121$ Da, CO_2CS $m/z= 44$ Da, BF_2 $m/z=49$ Da, HF $m/z=20$ Da) and recorded at a heating rate of $10^0C/min$ are given.

HF and BF_2 ($m/z=20$ and 49 Da respectively) due to evolution of dopant from PTh, and the thiophene trimer ($m/z=248$ Da) and H_2S ($m/z=34$ Da) due to degradation of polythiophene chains and cleavage of the thiophene ring recorded during the pyrolysis of mechanical mixture and electrochemically prepared P(TATE-co-Th). When the trends in the characteristics P(TATE) and dopant based peaks are considered, quite high resemblance to that of P(TATE-co-Th) is observed. Identical products having identical time-temperature resolved ion current profiles have been detected at both $19eV$ and $70eV$ revealing that the thermal degradation characteristics of P(TATE) and dopant are not affected by the presence of PTh significantly. The $19eV$ EI pyrolysis mass spectrometry results are in accordance with the $70eV$ EI results, except for the increase in relative intensities of products H_2S and H_2O . When the trends of thiophene based fragments were compared with those recorded from pure PTh, again quite similar trends were recorded indicating that thermal characteristics of PTh was not significantly affected by the presence of TATE. Present results reveal that polymerization of both TATE and Th occurred during the electrochemical process, yet the data is not sufficient to confirm copolymer formation.

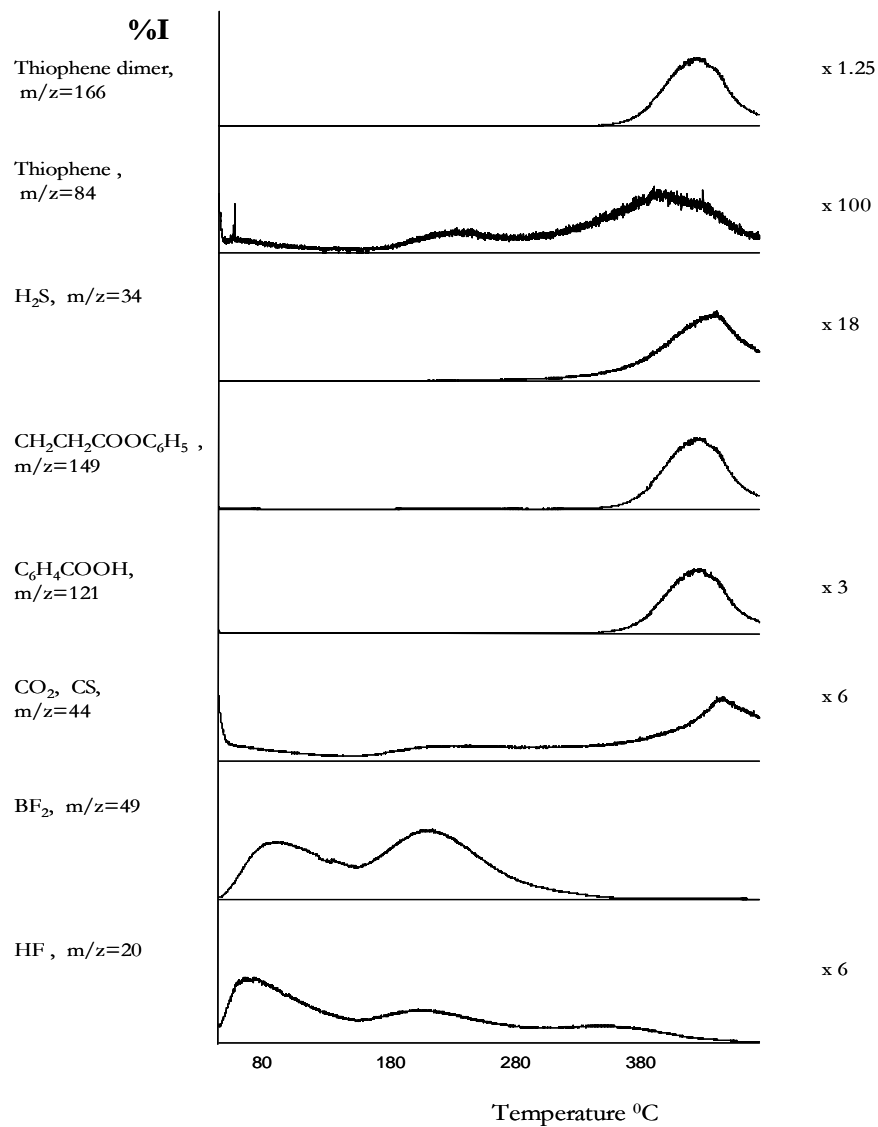


Figure 3.15 Single ion pyrograms of some selected fragments recorded during pyrolysis of P(TATE-co-Th)

3.1.4 Thermal Gravimetric Analysis of TATE

As shown in Figure 3.16.a, TGA curve of TATE showed single weight loss at 342°C. The TGA curve for homopolymer revealed two transitions at 81 °C and 412 °C, which can be attributed to the removal of solvent and decomposition respectively (Figure 3.16.b). The char residue of PTATE was 49 % after 630 °C. However, 2 % of TATE remained after 530 °C. In the case of copolymer, thermogravimetry scan showed weight loss at 82 °C due to entrapped solvent and monomer, at 235 °C due to the removal of dopant ion and at 407 °C due to decomposition (Figure 3.16.c) [55].

3.1.5 Conductivities of TATE

The conductivity of P(TATE) was measured as 4×10^{-5} S/cm according to four probe technique. For the copolymer with thiophene this value was determined to be 4×10^{-3} S/cm.

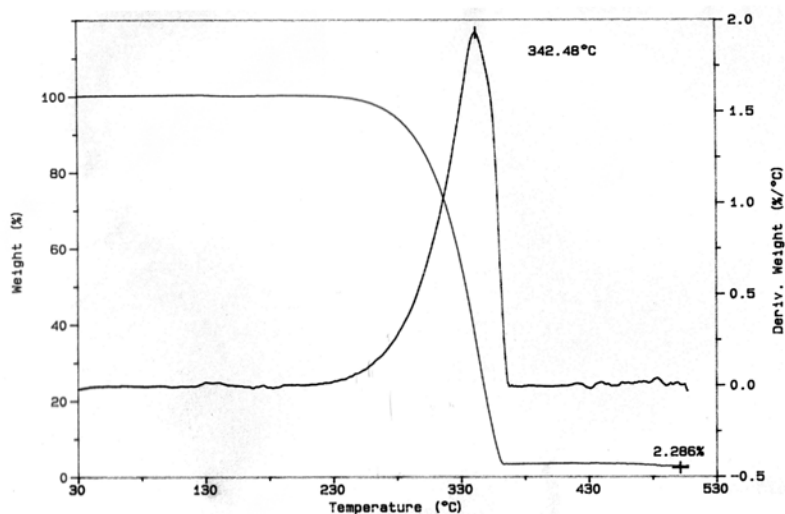


Figure 3.16.a TGA curve of TATE

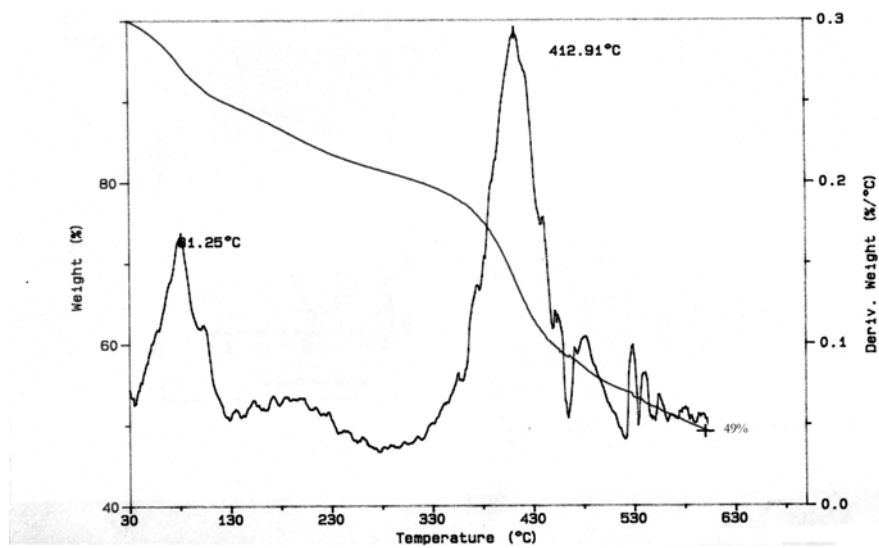


Figure 3.16.b TGA thermogram of P(TATE)

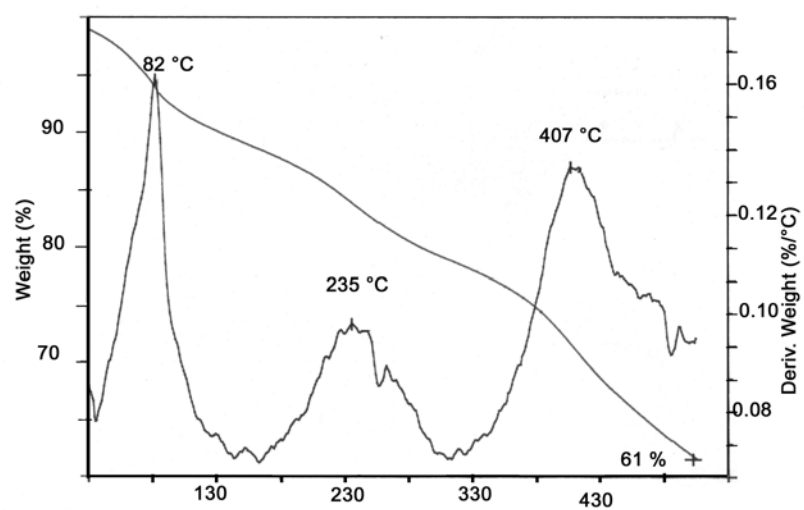


Figure 3.16.c TGA thermogram of P(TATE-co-Th)

3.3 OTE and Its Polymers

3.3.1 OTE

The mass spectrum of the monomer, OTE, was also recorded in the temperature range of 25°C-445°C. The peaks related to the monomer appeared in the pyrolysis mass spectra at initial stages of pyrolysis. Figure 3.17 shows the mass spectrum of the monomer recorded at 45°C. The intense and/or characteristic peaks observed in the mass spectrum are summarized in Table 7.

The detailed analyses of the mass spectra indicated that the fragmentation follows the classical ester degradation mechanism, together with long hydrocarbon chain and thiophene fragmentation patterns. The base peak at $m/z = 110$ Da is due to the McLafferty rearrangement reaction as shown in Scheme 8.

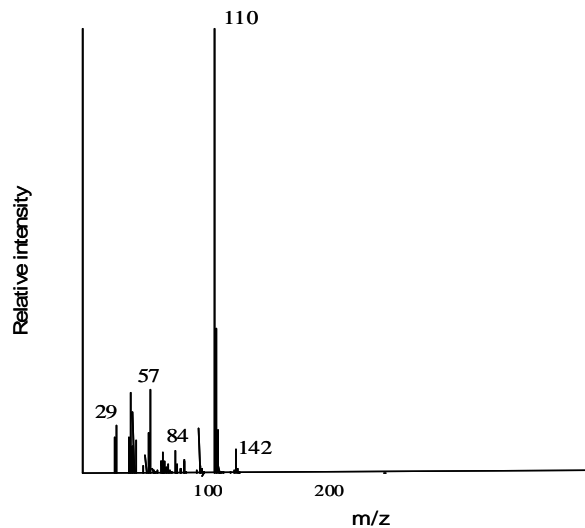
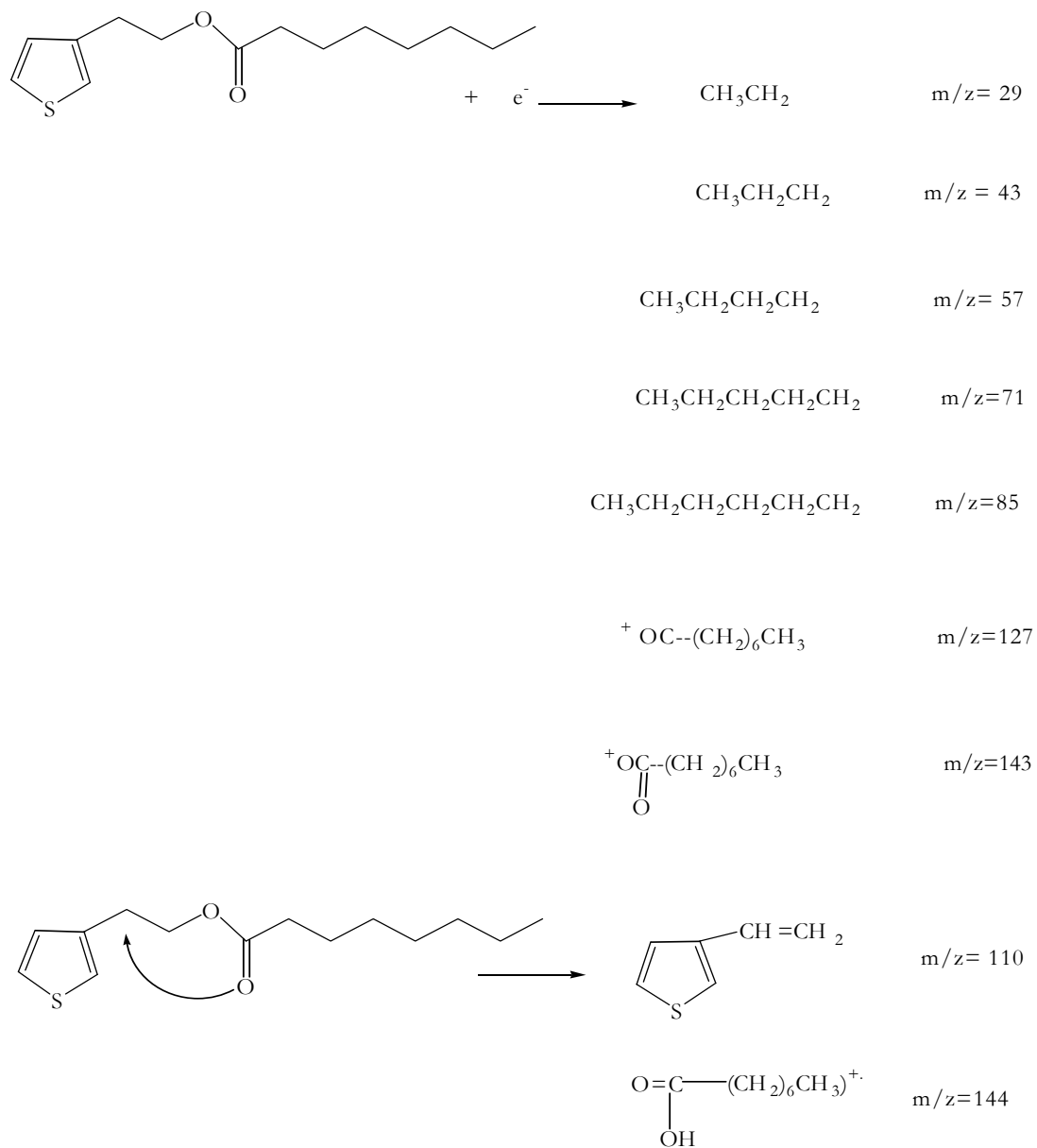


Figure 3.17 Mass Spectra of OTE



Scheme 8. Proposed degradation products of OTE

3.3.2 Homopolymer of OTE (P(OTE))

The total ion current (TIC) curve of P(OTE) shows two peaks with maxima at 40⁰C and 440⁰C. The TIC curve and the mass spectra recorded at these temperatures are given in Figure 3.18.

Analyses pointed out that the first maximum corresponds to the evolution of low molecular weight compounds such as H₂O, BF₃, C₃H₅, CHCO, C₄H₇. The mass spectrum recorded at 440⁰C showed that the peaks due to C₄H₁₂ (m/z=60 Da), C₄H₇ (m/z =55 Da), C₄H₃SCH₂ (m/z=97 Da) were the most intense ones. Furthermore, the monomer peak was also detectable. The characteristic and/or intense peaks in the pyrolysis mass spectra recorded at the maxima of the TIC curve are summarized in Table 7.

The detailed analyses of the mass spectra indicated that the fragmentation of the side chains of the polymer follows the classical ester fragmentation pattern as in the case of the monomer. Yet, the relative intensities of the product peaks changed significantly. In case of the monomer, the peak at m/z=110 Da due to the cleavage at α - position to the CO group is the base peak. However, for the polymer, the base peak at m/z=43 Da is due to the alkyl fragment due to the degradation of the side chains. The peak at m/z=110 Da is also present though relatively weak. Peaks due to H-transfer and McLafferty rearrangement reactions are also present in the spectra. Furthermore, thiophene peak is more intense for the POTE and weak dimer and trimer peaks are observable.

A great degree of similarity between the mass spectrum of the monomer and pyrolysis mass spectra of the corresponding polymer can be observed only if the thermal degradation proceeds through a depolymerization mechanism. In our case however, the

pyrolysis mass spectra of P(OTE) is totally different than the mass spectrum of the monomer.

The thermal degradation of polymers involving labile side chains usually starts with the cleavages of weak bonds substituted on the main chain. Thus, the monomer and oligomers peaks are either weak or absent in the pyrolysis mass spectra of such polymer. In any case we did not expect any similarity in the mass spectra of OTE and P(OTE).

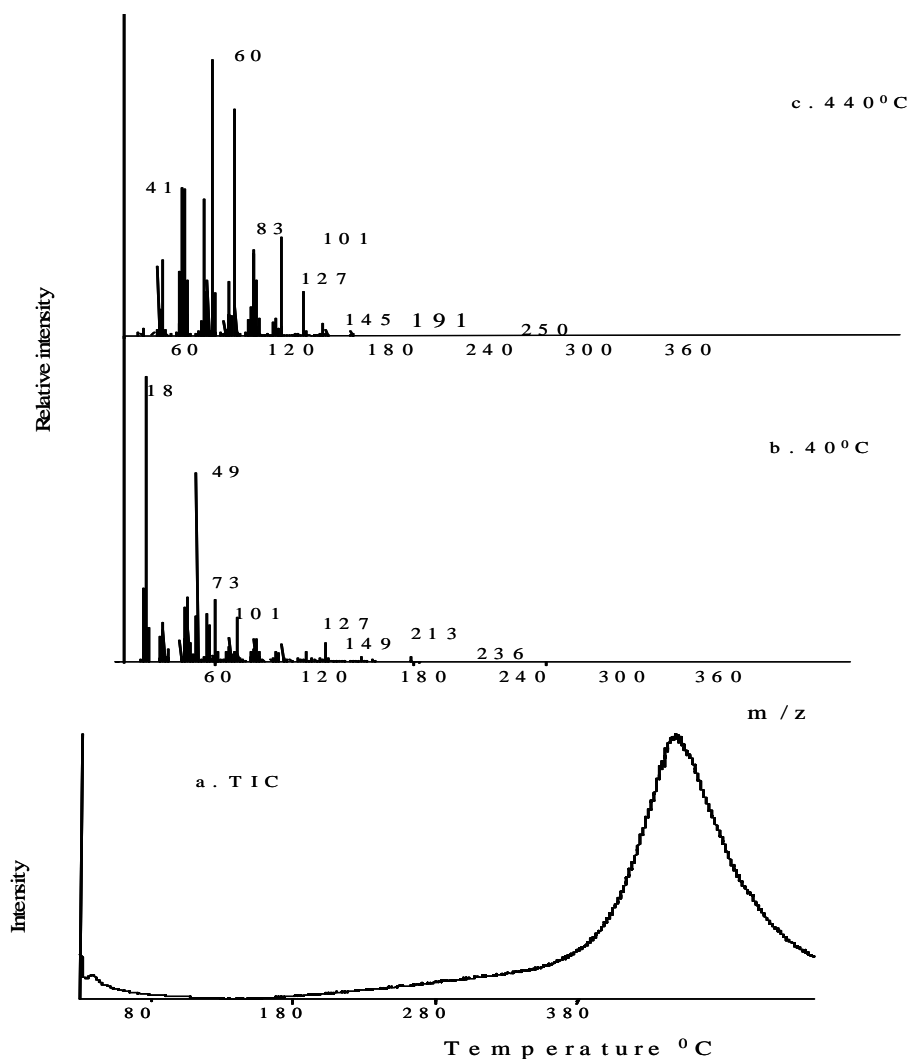


Figure 3.18 a. The TIC curve and the mass spectra recorded at b. 400C, c. 440 °C

Table 7 The most and/or characteristic peaks of OTE and P(OTE) at some selected temperatures, with related chemical formula

m/z	P(OTE)			OTE		Assignments	
	70 eV		19 eV				
	40°C	445°C		40°C	445°C		
18	1000	27		525	9	1	H ₂ O
28	125	92		100	39	127	N ₂ , CO, C ₂ H ₄
29	103	276		77	102	150	C ₂ H ₅
30	17	11		20	11	4	BF, CH ₂ =NH, CH ₂ =O
34		17			20		H ₂ S
39	64	237		14	13	98	C ₃ H ₃
41	168	540		202	258	197	CH ₃ CN, C ₃ H ₅
43	212	532		632	655	132	C ₃ H ₇
44	106	75		186	79	77	CO ₂ , CS
49	546	1		728	1		BF ₂
55	150	495		330	455	70	C ₄ H ₇
57	119	200		486	286	139	CHCS, C ₄ H ₉
60	177	1000		1000	1000	5	OCS, OHCOHCH ₂
68	45	21		95	22		BF ₃
73	140	816		732	889	3	C ₃ H ₅ S
84	64	297		364	417	31	C ₄ H ₃ S
97	32	48		92	77	78	C ₄ H ₃ SCH ₂
101	48	360		303	508	2	FC ₄ H ₂ S
110	11	5		40	7	1000	C ₄ H ₃ SCHCH ₂
127	69	47		542	60	32	OC(CH ₂) ₆ CH ₃
138	5	2		24	2	3	C ₃ H ₃ C ₄ H ₂ (OH)S
142	4	8		424	13	1	(C ₄ H ₉) ₂ N=CH ₂ , (C ₃ H ₃ S) ₂
143	5	5		69	6	1	OCO(CH ₂) ₆ CH ₃
155	6	1		13	1	5	OCOCH(CH ₂) ₅ CHCH ₂
166	2	1		14	1	2	C ₄ H ₃ SC ₄ H ₃ S
171	5	1		50	1	1	C ₄ H ₃ S(CH ₂) ₂ OCOHCH ₂
179	3	1		4	1	1	C ₄ H ₃ SC ₄ H ₂ SCH ₂
185	6	1		54	1		(C ₄ H ₉) ₃ N
207	2	1		1		6	C ₄ H ₃ SC ₄ H ₂ SCH ₂ CH ₂ CH ₂
242	1			72			(C ₄ H ₉) ₄ N
254	1			3		4	Monomer

The single ion current temperature profiles of important fragments of P(OTE) are shown in Figure 3.19. The peaks related to the anion of the supporting electrolyte such as BF_3 , BF_2 , BF and HF appeared at the first stage of pyrolysis. Therefore, the evolution of the supporting electrolyte was considered at this region. The peaks at $m/z=83$, 73, 60 and 57 Da due to thiophene, $\text{CH}_2\text{OC}(\text{OH})=\text{CH}_2$, $\text{HOC}(\text{OH})=\text{CH}_2$ and C_4H_9 appeared respectively in pyrolysis mass spectra in the same temperature ranges and their evolution profiles were quite similar. Similar fragments to PTh were recorded; polymerization through the thiophene moieties was concluded to be successful. The relative yield of H_2S was quite low. Previous studies showed that H_2S evolution, indicating cleavage of the thiophene ring is more likely when a network structure exists. Thus, it may be concluded that extent of network structure is quite low [60].

In order to limit the further dissociation of degradation products in the mass spectrometer, the pyrolysis experiments were also performed decreasing ionization energy to 19 eV. Yet, no significant change in fragmentation pattern was observed. Thus, it can be concluded that secondary ionization was not very important.

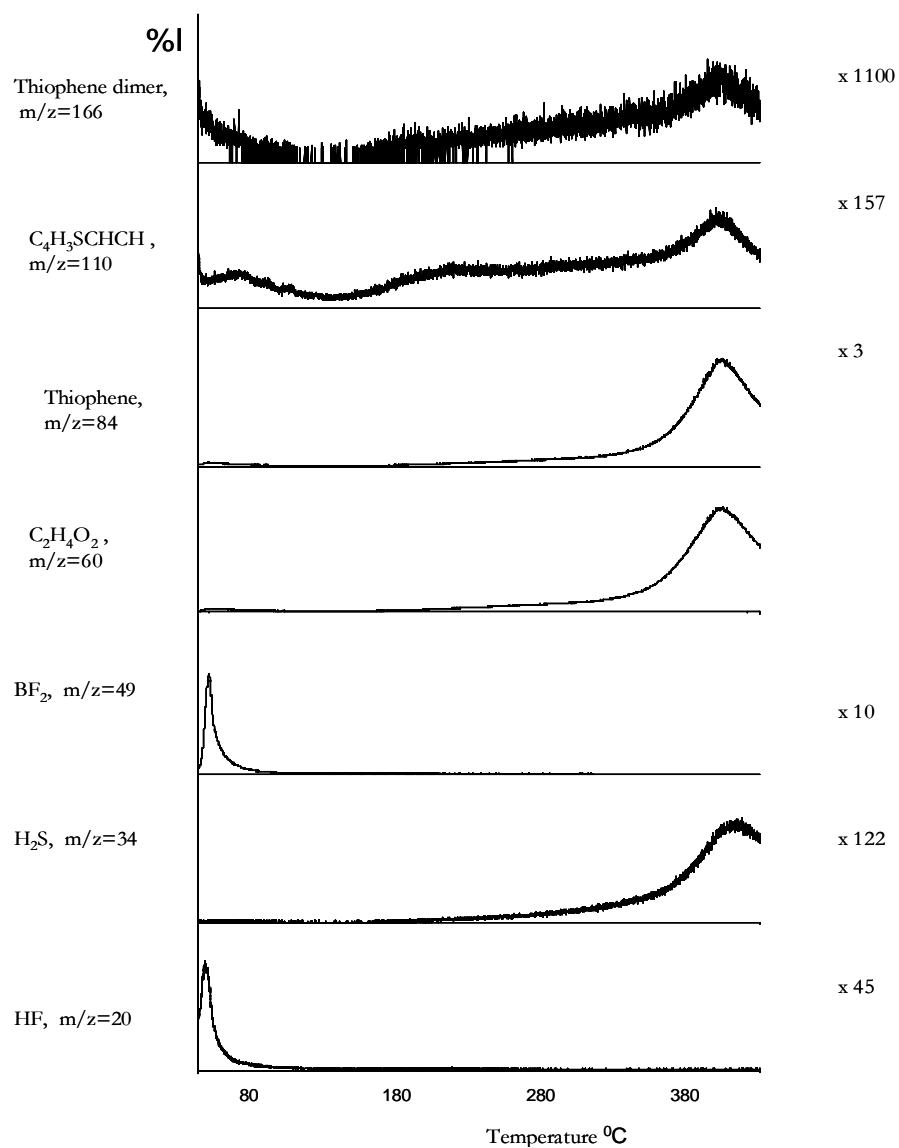


Figure 3.19 The ion-temperature profiles of most intense and characteristic peaks as a function of temperature observed during pyrolysis of P(OTE)

3.3.3 Copolymer of OTE with Thiophene (P(OTE-co-Th))

The decomposition of P(OTE-co-Th) occurred in a broad temperature range as shown in Figure 3.21. Two weak low temperature peaks and a broad intense peak were observed in the total ion current (TIC) curve. This type of a profile indicates either a multi step degradation mechanism or presence of many components in the sample under investigation. In Figure 3.20 the TIC curves for POTE, PTh, mechanic mixture of POTE and PTh and P(OTE-co-Th) are shown for comparison. It is observed from Figure 3.18 that the TIC curves of all the samples show different trends. Analyses of the pyrolysis mass spectra recorded at the maximum of the peaks in the TIC curve of P(OTE-co-Th) pointed out that the first two maxima correspond to the evolution of low molecular weight compounds such as H_2O , BF_3 , C_2H_5 and C_3H_7 . In the temperature range 200-300°C peaks due to TBAFB were also observed. In the last stage of the pyrolysis, the monomer and low molecular weight oligomer peaks appeared in the mass spectra. The characteristic and/or intense peaks in the pyrolysis mass spectra recorded at the maxima of the TIC curve are summarized in Table 8.

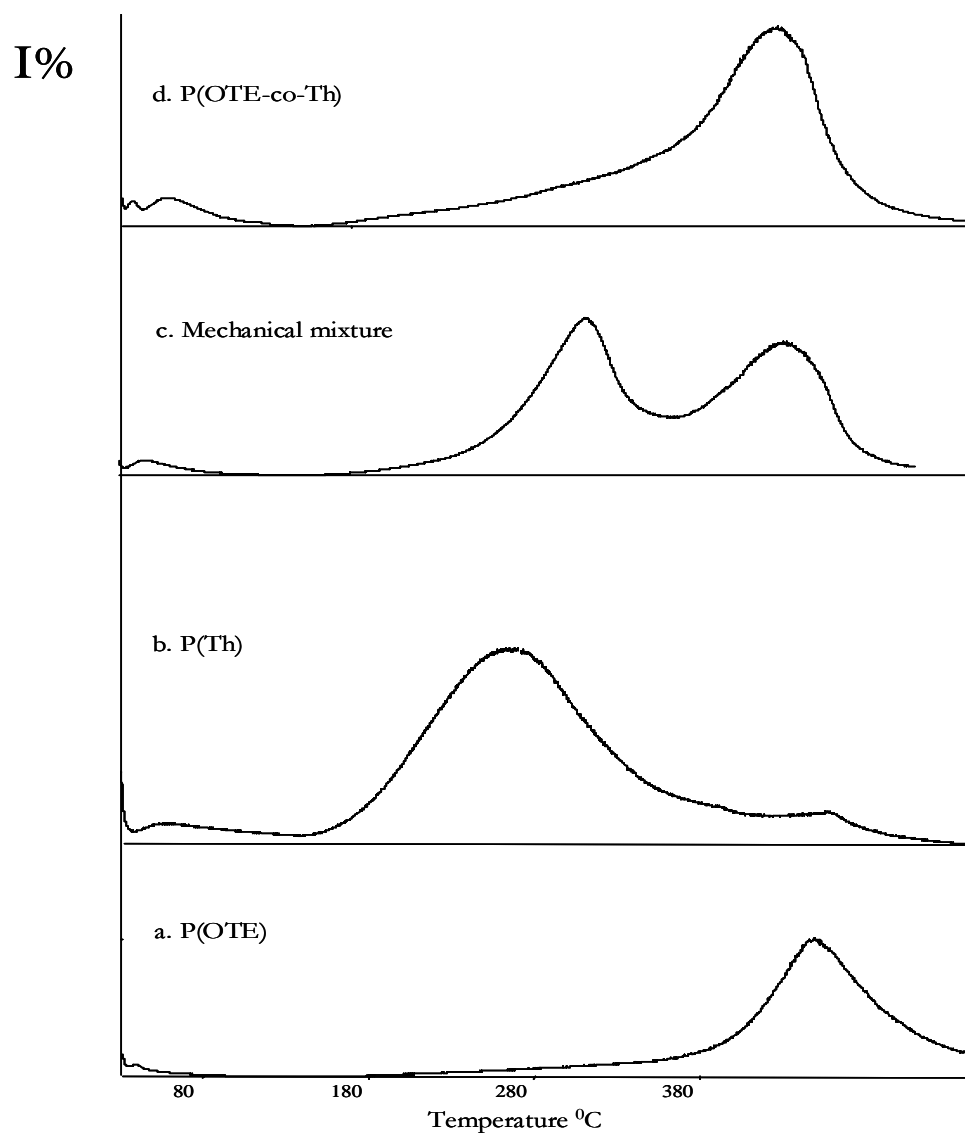


Figure 3.20 TIC curve recorded during the pyrolysis of a. P(OTE), b. P(Th), c. mechanical mixture and d. P(OTE-co-Th)

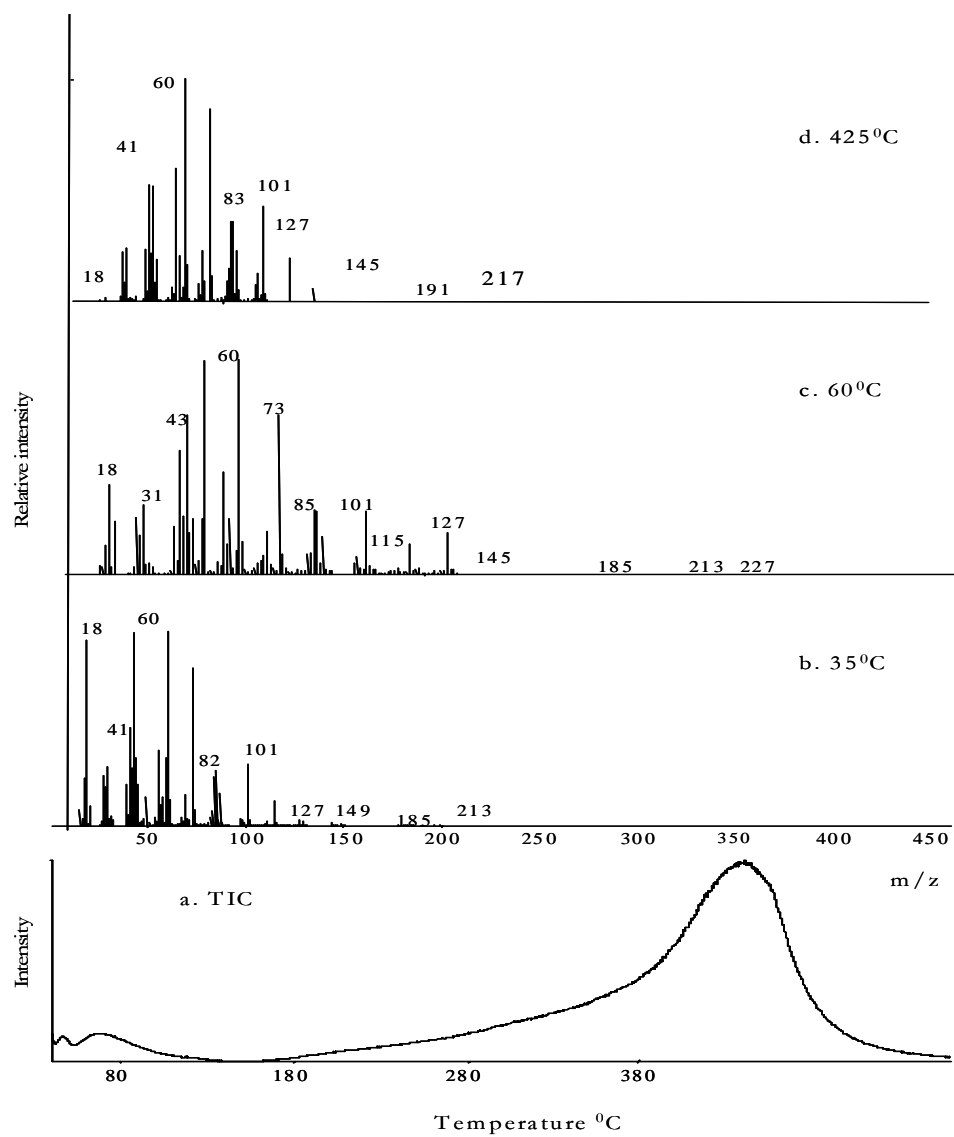


Figure 3.21 a. The TIC curve and the mass spectra recorded at b. 35 °C, c. 60 °C, d. 425°C

The time-temperature resolved evolution profiles of P(OTE-co-Th) based ions are given in Figure 3.22. As shown in Figure 3.20, the evolution profiles of P(OTE) based fragments followed almost the same trends when generated from the copolymer. The relative intensity of dopant based peaks was stronger in the pyrolysis mass spectra of the copolymer compared to POTE but weaker compared to PTh. Again, the intensities of the peaks due to PTh based products especially H_2S were higher in the pyrolysis spectra of the copolymer compared to POTE. This indicates the cleavages of the thiophene rings of polymer chains involving a crosslinked structure. However, the main degradation products of P(OTE-co-Th) due to loss of side chains confirms the presence of both P(OTE) and PTh units in the copolymer.

All these results confirm that the P(OTE-co-Th) sample contains chains showing characteristic thermal degradation patterns of PTh and POTE, no direct support for copolymerization can be determined.

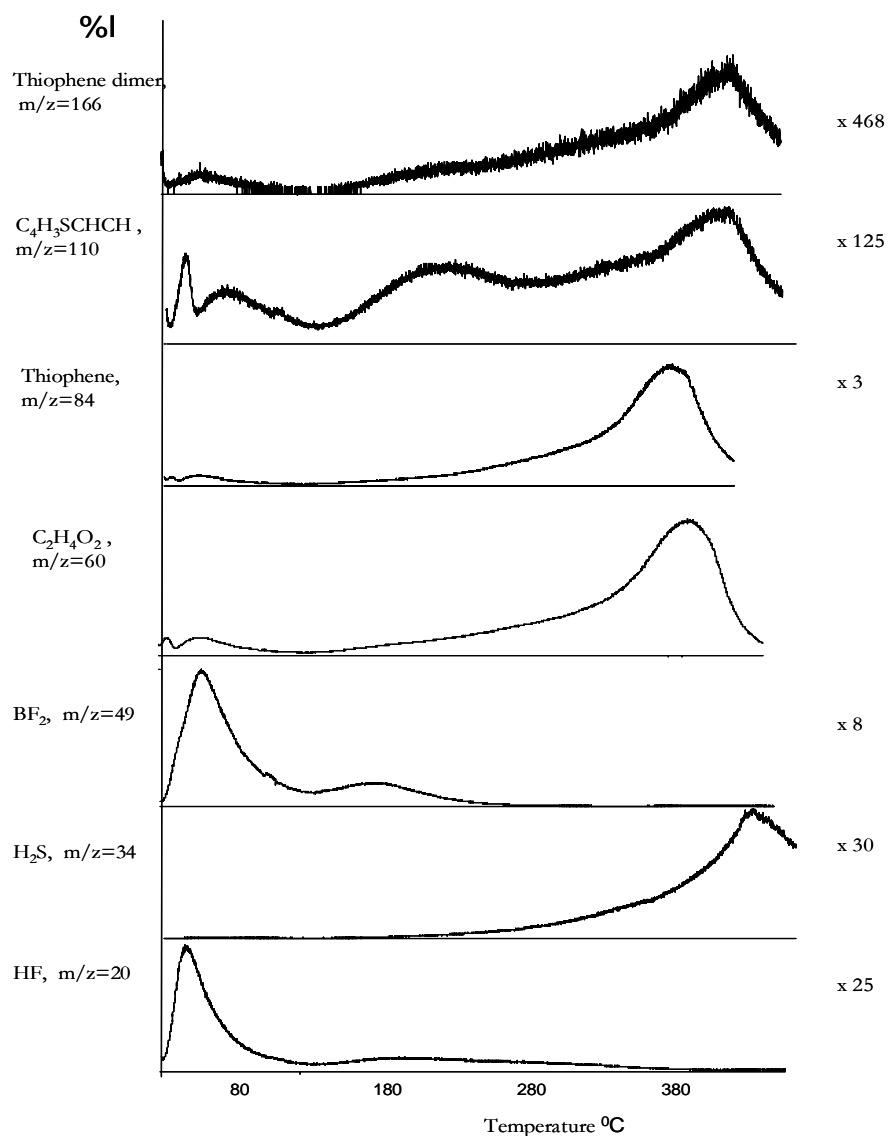


Figure 3.22 Single ion pyrograms of some selected fragments recorded during pyrolysis of P(OTE-co-Th)

Table 8 The most and/or characteristic peaks of P(OTE-co-Th) at some selected temperatures, with related chemical formula

m/z	P(OTE-co-Th)				Assignments		
	70 eV		19 eV				
	30°C	70°C	425°C	50°C	275°C	425 °C	
18	964	411	19	393	3	9	H ₂ O
28	192	179	87	77	8	34	N ₂ , CO, C ₂ H ₄
29	304	321	237	54	15	71	C ₂ H ₅
30	41	42	12	146	12	7	BF, CH ₂ =NH, CH ₂ =O
39	209	225	235	25	6	22	C ₃ H ₃
41	513	577	520	138	55	226	CH ₃ CN, C ₃ H ₅
43	961	726	521	690	52	480	C ₃ H ₇
44	337	182	86	344	58	61	CO ₂ , CS
49	146	1000	1	12	751	1	BF ₂
55	375	461	590	215	40	396	C ₄ H ₇
57	147	254	205	375	51	204	CHCS, C ₄ H ₉
60	1000	998	1000	599	120	1000	OCS, OHCOHCH ₂
68	25	87	33	119	3	20	BF ₃
73	807	743	868	529	89	806	C ₃ H ₅ S
84	255	292	359	289	45	313	C ₄ H ₃ S
97	37	55	74	117	6	61	C ₄ H ₃ SCH ₂
101	303	295	427	207	59	365	FC ₄ H ₂ S
110	14	19	8	123	2	8	C ₄ H ₃ SCHCH ₂
115	123	136	198	103	16	153	
127	33	176	59	465	5	48	OC(CH ₂) ₆ CH ₃
138	3	4	3	33	1	3	C ₃ H ₃ C ₄ H ₂ (OH)S
142	2	5	5	118	1000	17	(C ₄ H ₉) ₂ N=CH ₂ , (C ₃ H ₃ S) ₂
143	3	8	5	47	120	5	OCO(CH ₂) ₆ CH ₃
155	1	3	2	22	1	1	OCOCH(CH ₂) ₅ CHCH ₂
166	1	2	2	20	1	2	C ₄ H ₃ SC ₄ H ₃ S
171	3	5	2	89	2	1	C ₄ H ₃ S(CH ₂) ₂ OCOHCH ₂
179	1	2	2	16	1	2	C ₄ H ₃ SC ₄ H ₂ SCH ₂
185	3	2	1	17	86	1	(C ₄ H ₉) ₃ N
191	1	2	2	9	1	1	C ₄ H ₃ SC ₄ H ₂ SC ₂ H ₂
242	1	1	1		27	1	(C ₄ H ₉) ₄ N
254			1	8	1	1	Monomer

3.3.4 Thermal Gravimetric Analysis of OTE

The homopolymer of OTE showed single step decomposition at 415 °C, leaving 23.05% residue. Since degree of doping was too low, removal of the dopant anions from the matrix, leading to a significant weight loss might not be observed (Figure 3.23.c). TGA thermogram of the copolymer P(OTE-co-Th) revealed two weight losses at 203°C and 414°C, which could be attributed to the removal of dopant anion from the matrix and decomposition of the polymer itself respectively (Figure 3.23.a). Although both the PTh and P(OTE-co-Th) exhibited two step decomposition, both the dopant removal and decomposition of the polymer matrix were very different from each other [57].

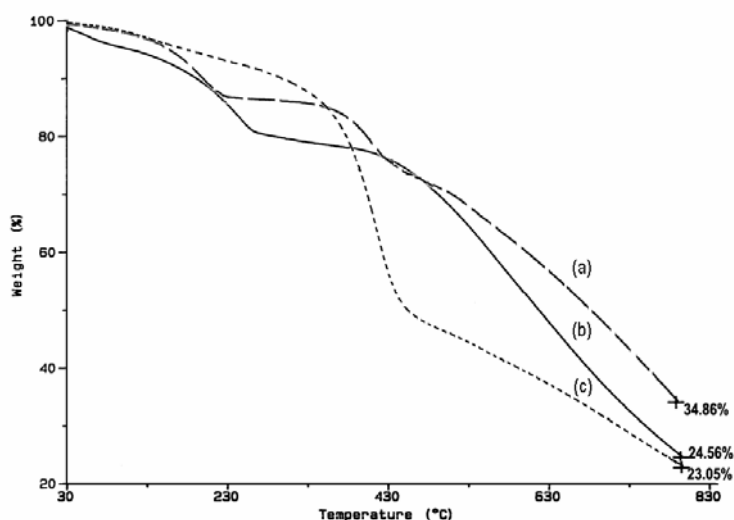


Figure 3.23 TGA thermogram of potentiostatically synthesized (a) P(OTE-co-Th) (b) P(Th) (c) P(OTE)

3.3.5 Conductivity Measurements of OTE

Conductivity of P(OTE) and P(OTE-co-Th) were 3.2×10^{-4} , 9.1×10^{-2} S/cm respectively.

CHAPTER 4

CONCLUSIONS

In this study, terephthalic acid bis-(2-thiophen-3-yl-ethyl)ester (TATE), decanedioic acid bis-(2-thiophen-3-yl-ethyl) ester (DATE) and octanoic acid 2-thiophen-3-yl-ethyl ester (OTE), their corresponding homopolymers have been prepared electrochemically. Electrochemical polymerizations of TATE, DATE and OTE have been performed in solutions containing thiophene to prepare copolymers of these thiophene derivatives.

- Direct pyrolysis mass spectrometry analyses of electrochemically polymerized P(DATE) revealed that the growth of polymer occurred through both 2 and 5 positions. On the other hand, it is determined that P(TATE) polymerized through 5 position yields a polymer with a lower conductivity.
- For all the polymers under investigation, evolution of dopant occurred at two temperature ranges. Evolution of BF_3 at initial stages below 100°C was attributed to adsorbed supporting electrolyte whereas dopant leaves the polymer matrix at around 230°C . For the samples, the relative intensities of dopant based peaks were low compare to that of polythiophene based peaks. Furthermore, the relative yield of H_2S was quite low for these polymers. Previous studies shown that H_2S evolution, indicating cleavage of the thiophene ring is more likely when there exits a network structure. Thus, it may be concluded that the extent of network structure is quite low for the derivatives.

- Pyrolysis of all the samples prepared by electrochemical oxidation of DATE, TATE or OTE in the presence of Th, yielded characteristic fragments of both homopolymers and polythiophene units confirming copolymerization.
- Similar thermal characterization were recorded indicating that thermal units were not significantly affected by the presence of TATE, DATE or OTE. Present results reveal that polymerization of OTE or TATE with Th occurred during the electrochemical process, yet the data is not sufficient to confirm copolymer formation.
- Pyrolysis of the polymer sample prepared by electrochemical oxidation of DATE and Th indicated the presence of low molecular weight DATE oligomers. This may be attributed to growth of thiophene through DATE confirming copolymer formation.

Papers in International Journals:

- E.Aslan, P.Camurlu, L.Toppare, ‘Synthesis and Electrochromic Properties of A Symmetric Thiophene Derivative: Decanedioic Acid Bis-(2-Thiophen-3-yl-ethyl)ester and Its Copolymer with Thiophene” *J.Macr.Sci. Pure and Appl Chem.* (*in press 2004*)
- E.Aslan, J.Hacaloglu, L.Toppare, “Investigation of The Effect of Substituent on The Growth of Polymer for 3-Substituted Polythiophenes Via Pyrolysis Mass Spectrometry” *Synth. Met.*(*submitted 2004*)

REFERENCES

1. J. D. Stenger-Smith, *Prog. Polym. Sci.*, 23, 53, 1998
2. H. A. Pohl, *Chem Eng.*, 68 (22), 105, 1961
3. J. E. Katon and B.S. Wildi, *J. Chem. Phys.*, 40(10), 2977, 1964
4. H. A. Pohl and E. H. Engelhardt, *J. Phys. Chem.*, 66, 2085, 1962
5. F. B. Burt, *J. Chem. Soc.*, 1171, 1910
6. G. MacDiarmid, *J. Am. Chem. Soc.*, 98, 3884, 1976
7. M. Akta, et al., *J. Chem. Soc. Chem. Commun.*, 846, 1977
8. H. Shirakawa, E. J. Louis, A. G. MacDiarmid, C. K. Chiang and A. J. Heeger, *J. Chem. Soc., Chem. Commun.*, 578, 1977
9. T. Ito, H. Shirakawa and S. Ikeda, *J. Polym. Sci. Polym. Chem. Ed.*, 12, 11, 1978
10. C. K. Chiang, Y. W. Park, A. J. Heeger, H. Shirakawa, E. J. Louis and A. G. MacDiarmid, *J. Chem. Phys.*, 69, 5098, 1978
11. P. J. Nigrey, A. G. MacDiarmid and A. J. Heeger, *J. Chem. Soc., Chem. Commun.*, 594, 1979
12. D. Jr. MacInnes, M. A. Druy, P. J. Nigrey, D. P. Nairns, A. G. MacDiarmid and A. J. Heeger, *J. Chem. Soc., Chem. Commun.*, 317, 1981
13. J. Heinze, *Syn. Met.*, 41-43, 2805, 1991
14. J. Heinze, *Top. Curr. Chem.*, 152,2, 1990
15. F. Diaz, K. K. Kanazawa and G. P. Gardini, *J. Chem. Soc., Chem. Commun.*, 635, 1979
16. G. Tourillon and F. Garnier, *J. Electroanal. Chem.*, 135, 173, 1982
17. F. Diaz and J. A. Logan, *J. Electroanal. Chem.*, 111, 111, 1980

18. Handbook of the Conducting Polymers, Vol 1, K. Doblhofer and K. Rajeshwar, edited by R. L. Elsenbaumer, R. J. Reynolds and T. A. Skotheim, Marcel Dekker Inc., USA
19. S. Sadki, P. Schottland, N. Brodie and G. Sabouraud, *Chem. Soc. Rev.*, 29, 283, 2000
20. E. M. Genies, G. Bidan and A. F. Diaz, *J. Electroanal. Chem.*, 149, 101, 1983
21. R. J. Waltman and J. Bargon, *Tetrahedron*, 40, 3963, 1984
22. D. J. Waltson, *Mater. Des.*, 11(3), 142, 1990
23. Electrical and Electronic Properties of Polymers: A State of the Art Compendium, Encyclopedia Reprint Series, John Wiley & Sons, NY
24. Alan McDiarmid, *Angew. Chem. Int. Ed.*, 40, 2581, 2001
25. J. L. Bredas, R. R. Chance and R. Silbey, *Phys. Rev.*, Part B., B26 (10), 5843, 1982
26. B. R. Weinberger, E. Ehrenfreund, A. J. Heeger and A. G. MacDiarmid, *J. Chem. Phys.*, 72, 4749, 1980
27. J. B. Goldberg, H. R. Crowe, P. R. Neuman, A. J. Heeger and A. G. MacDiarmid, *Mol. Cryst. Liq. Cryst.*, 72, 253, 1981
28. A. R. Bishop, D. K. Campbell and K. Fesser, *Mol. Cryst. Liq. Cryst.*, 77, 253, 1980
29. R. Qian and J. Qiu, *Polym. J.*, 19, 157, 1987
30. J. Roncali, F. Garnier, M. Lemaire and R. Garreau, *Synth. Met.*, 15, 323, 1986
31. Handbook of the Conducting Polymers, Vol 1, A. F. Diaz and J. Bargon, edited by T. J. Skotheim, Marcel Dekker Inc., USA
32. J. Roncali, *Chem. Rev.*, 92(4), 711, 1992
33. D. Zhang, J. Qin, G. Xue, *Synthetic Metals*, 100, 1999
34. G. Shi, S. Jin, G. Xue, C. Li, *Science*, 267, 1995
35. N. C. Billingham, P. D. Calvert, P. J. S. Foot and F. Mohammed, *Polym. Degrad. Stab.*, 19, 323, 1987
36. Y. Li and R. Quian, *Synth. Met.*, 53, 149, 1993
37. P. J. Nigrey, D. MacInnes, P. Nairns, A. G. MacDiarmid and A. J. Heeger, *J. Electro-chem. Soc.*, 128, 1651, 1981

38. Kitani, M. Kaya and K. Sasaki, *J. Electrochem. Soc.*, 133, 1069, 1986
39. J. H. Kaufman, T.C. Chun, A. J. Heeger and F. Wudl, *J. Electrochem. Soc.*, 131, 2092, 1984
40. R. Bittehn, G. Ely, F. Woelfler, H. Münstedt, H. Naarman and D. Naegelé, *Makromol. Chem., Macromol Symp.*, 8, 51, 1987
41. T. Nakajima and T. Kawagoe, *Synth. Met.*, 28, C629, 1989
42. O. Inganäs and I. Lundström, *Synth. Met.*, 21, 13, 1987
43. T. Kobayashi, H. Yoneyama and H. Tamura, *J. Electroanal. Chem.*, 161, 419, 1984
44. Çirpan, A. Avni Argun, Christophe R.G. Grenier, Benjamin D. Reeves, John R. J Reynolds, *Mater. Chem*, 13, 2422-2428, 2003
45. S. Alkan, A. C. Cutler, J. R. Reynolds, *Adv. Func. Mater.* 13, 4, 2003
46. J. Heinze and M. Dietrich, *Synth. Met.*, 41-43, 503, 1991
47. H. S. White, G. P. Kittlesen and M. S. Wrighton, *J. Am. Chem. Soc.*, 106, 5375, 1984
48. J. W. Thackeray and M.S. Wrighton, *J. Phys. Chem.*, 90, 6674, 1986
49. H. W. Meyer, K. Kiess, B. Binggelli, E. Meier and G. Harbeke, *Synth. Met.*, 10, 255, 1985
50. T. Uyar, L. Toppare and J. Hacaloğlu, *Synth. Met.*, 123, 335, 2001
51. T. Uyar, L. Toppare and J. Hacaloğlu, *Synth. Met.*, 119, 307, 2001
52. Mass Spectrometry, James Baker, edited by David J. Ando, John Wiley & Sons, USA
53. Ghassempour, N.M. Najafi, A.A. Amiri, *J. Anal. Appl. Pyrolysis*, 70, 251, 2003
54. S. M. Badawy, *Rad. Phys. Chem.*, 61, 143, 2001
55. Y. Coskun, A. Çirpan, L. Toppare, *Polymer*, 45(15), 4989, 2004
56. E. Aslan, P. Camurlu, L. Toppare, *J. Macro. Chem*, 2004 (in press)
57. P. Camurlu, A. Çirpan, L. Toppare, *Mater. Chem. Phys.*, 2004 (in press)
58. T. Uyar, L. Toppare, and J. Hacaloğlu, *Synth. Met.*, 119, 307, 2001
59. Y. Cao, P. Wang and R. Quian, *Macromol. Chem.*, 186, 1093, 1985
60. T. Gozet, A.M. Onal, J. Hacaloglu, *Synth. Met.*, 123, 335, 2001

